
DIGITAL ACCESS TO SCHOLARSHIP AT HARVARD
DASH.HARVARD.EDU

HARVARD LIBRARY


MITOCHONDRIAL TRANSPLANTATION AS A NOVEL THERAPEUTIC STRATEGY FOR RETINAL ISCHEMIA-REPERFUSION INJURY

Citation
Rubio Mijangos, Fernando. 2025. Mitochondrial Transplantation as a Novel Therapeutic Strategy for Retinal Ischemia-Reperfusion Injury. Masters Thesis, Harvard Medical School.

Link
https://dash.harvard.edu/handle/1/42719897

Terms of use
This article was downloaded from Harvard University's DASH repository, and is made available under the terms and conditions applicable to Other Posted Material (LAA), as set forth at
https://harvardwiki.atlassian.net/wiki/external/NGY5NDE4ZjgzNTc5NDQzMGIzZWZhMGFlOWI2M2EwYTg

Accessibility
https://accessibility.huit.harvard.edu/digital-accessibility-policy

Share Your Story
The Harvard community has made this article openly available.
Please share how this access benefits you. Submit a story

MITOCHONDRIAL TRANSPLANTATION AS A NOVEL THERAPEUTIC STRATEGY FOR RETINAL ISCHEMIA-REPERFUSION INJURY

by

Fernando Rubio-Mijangos, M.D.

A Dissertation Submitted to the Faculty of Harvard Medical School

in Partial Fulfillment of

the Requirements for the Degree of Master of Medical Sciences in Clinical Investigation (MMSCI)

Harvard University

Boston, Massachusetts

March, 2025

Area of Concentration: Ophthalmology

Project Advisors: James D. McCully, PhD and Demetrios Vavvas, M.D, PhD

I have reviewed this thesis. It represents work done by the author under my guidance/supervision:

Primary Mentors: James D. McCully, PhD and Demetrios Vavvas, M.D, PhD

Table of Contents

1. Acknowledgements …… 3

3. Thesis Overview and Abstract 6

2.Introduction ……9

3. Methods …… 15

4. Results 23

5. *Discussion*..... 32

6. *Conclusion* 49

7. *Limitations and Future Directions*..... 51

8. *Bibliography* 55

9. *Figures* 62

Acknowledgements

I would like to express my deepest gratitude to **Dr. James D. McCully** for opening the doors of his lab to me and for having the patience to introduce me to the intricate world of mitochondria. His unwavering support has fueled my passion for this field, constantly pushing me to strive for nothing less than excellence. I am incredibly grateful for the countless hours of guidance and feedback, for the many anecdotes shared, and for his dedication to my growth. His mentorship has been invaluable, and I will carry the lessons he has taught me throughout my career. I would also like to extend my sincere appreciation to **Dr. Aybüke Çelik** for her patience and support in guiding me through study design and methodology. Her rigorous approach has given me something to aspire to, setting an example of excellence for the next generation of scientists.

I am equally grateful to **Dr. Demetrios Vavvas** for demonstrating the highest standards in research and for showing me the immense potential of translational science, especially in the field of ophthalmology. His support at every step of this journey has been a source of strength and motivation. I deeply appreciate his curiosity and open-minded approach, which have inspired me to think critically and innovatively. His guidance has shaped my understanding of the broader impact of research, and I am truly fortunate to have had him as a mentor.

To **Dr. Carmen Clapp** for introducing me to the world of research. She was the first to believe in me, to guide me in retinal studies, and to fuel my passion for science. Her support and mentorship shaped my journey, and I am forever grateful for the foundation she helped me build.

Thank you as well to **Dr. Martin Picard**, who unknowingly got me into the world of mitochondria, his commitment to their study and diffusion has been invaluable and truly inspiring.

To my program directors, **Dr. Martina McGrath, Dr. Rosalyn Adam, and Dr. Finnian McCausland**, I extend my highest gratitude for your tremendous teaching, invaluable guidance, and unwavering support. Your mentorship has been instrumental in ensuring my work speaks for itself, meets the highest quality standards, and reflects scientific rigor. You have not only followed up on my progress but have also inspired me to embrace a multidisciplinary approach, strengthening my ability to navigate complex scientific and clinical landscapes. Thank you for never doubting my potential, for always steering me in the right direction, even when I veered off course, and for shaping both this project and my growth as a professional.

A special thank you to **Dr. María Loscertales**, for coaching me not only as a professional but also as a person, for her unwavering support, leadership, and encouragement. Thank you for sharing my enthusiasm for this project, for always seeking new knowledge alongside me, and for helping me become a better scientist and individual every step of the way.

I would like to express my highest gratitude to my dad **Santiago Rubio**, my friends **Alejandro Montaudón, José Luis Vázquez, Alan Christensen, Antonio Granados, and Francisco Ortega,** as well as to my sister **Ariadna Rubio-Mijangos,** for their unwavering support throughout this journey. Thank you for being there during the challenging moments, for your laughter, advice, constant help, and most of all, for always keeping me smiling, strong, and eager to grow. Your presence has been a fundamental pillar in my life now and always, and key in the completion of this project. Finally, my greatest of gratitude and dedication go to my mother, **Alicia Mijangos**, whose love and unwavering support have been my greatest motivation. She asked every

day about my progress, showing a genuine curiosity and pride that fueled my perseverance. More importantly, she taught me what it means to be human, to be kind, curious, positive-minded, to follow my wildest dreams no matter the obstacles, and to always rise after every fall. And, of course, thank you mom for giving me my mitochondria, that have fueled this entire journey!

Thesis Overview

Title: Mitochondrial Transplantation as a Novel Therapeutic Strategy for Retinal Ischemia-Reperfusion Injury

Authors: Fernando Rubio-Mijangos[1,2], Aybuke Çelik[1], Maria Loscertales[2], Alexander Bigger-Allen[3], Sitaram Emani[1], Pedro del Nido[1], Demetrios Vavvas[2*], James D. McCully[1*]

[1]Department of Cardiac Surgery, Boston Children's Hospital, Department of Surgery, Harvard Medical School, Boston, MA, 02215, USA

[2]Department of Ophthalmology, Retina Service, Massachusetts Eye and Ear, Harvard Medical School, Boston, MA 02114, USA

[3]Urological Diseases Research Center, Boston Children's Hospital, Harvard Medical School, Boston, MA 02114, USA

*Co-last authors

Keywords: Mitochondrial transplantation; Retinal ischemia-reperfusion injury; Oxidative stress; Mitochondrial dysfunction; Cellular bioenergetics; ARPE-19; Inflammation; Apoptosis;

Abstract Word Count: 322

Word Count: 11367

Abstract

Background

Mitochondria are central to cellular homeostasis, providing ATP through oxidative phosphorylation while also regulating oxidative stress, apoptosis, and immune responses. Retinal ischemia-reperfusion injury (RIRI) disrupts mitochondrial function, triggering oxidative stress, inflammation, and neurovascular degeneration. Given the critical role of mitochondria in retinal cell survival, mitochondrial transplantation (MT) has emerged as a promising therapeutic strategy to restore mitochondrial integrity and bioenergetics in ischemic tissues. This study evaluates the potential of MT in rescuing oxidative stress-induced mitochondrial dysfunction in an in vitro model of RIRI.

Methods

ARPE-19 cells were differentiated into a mature retinal pigment epithelium-like phenotype and subjected to oxidative stress using hydrogen peroxide (H_2O_2). Mitochondria were isolated from ARPE-19 cells and characterized for viability and function. Transplantation was performed at optimized doses, and mitochondrial uptake, ATP production, oxidative stress resilience, and cell survival were assessed. Bulk RNA sequencing was conducted to analyze transcriptional responses following MT, identifying differentially expressed genes and enriched biological pathways involved in cellular stress adaptation.

Results

Transplanted mitochondria were efficiently internalized by ARPE-19 cells and integrated into the host mitochondrial network, restoring ATP levels in a dose-dependent manner. MT significantly improved cell survival and reduced oxidative stress-induced apoptosis at 0.25-0.5 mM H_2O_2 concentrations. RNA sequencing revealed that MT downregulated inflammatory and apoptotic pathways, including IL-17, VEGF, and CASP9 signaling, while upregulating stress-adaptive pathways such as TNF, NF-κB, SGK1, and efferocytosis. Notably, MT reduced IL6 and IL6R expression, potentially mitigating inflammation-driven mitochondrial dysfunction.

Conclusion

MT demonstrates significant potential in restoring mitochondrial function and modulating stress-responsive transcriptional programs in RIRI models. By mitigating oxidative stress, preserving ATP levels, and reprogramming inflammatory responses, MT presents a promising therapeutic approach for retinal ischemic diseases.

Future Directions

Further investigations are required to validate these findings in vivo, refine transplantation protocols, and assess the long-term efficacy and safety of MT. Proteomic and metabolomic analyses could provide deeper insights into mitochondrial integration and functional recovery, advancing MT as a viable intervention for retinal ischemia.

Introduction

Mitochondria are often called the powerhouses of the cell for their ATP-generating capacity, but they fulfill many other vital functions that influence cell and tissue homeostasis. Far from being mere energy suppliers, mitochondria actively partake in hormonal regulation, immune signaling, secretory processes, cell survival pathways, and apoptosis. Recent advances have reshaped our understanding of mitochondria, emphasizing their role as dynamic information processors, far beyond their metabolic functions. Rather than static organelles, mitochondria have been described to integrate signals, and generate outputs that shape cellular and even systemic physiology(1), maintaining mitochondrial function supports cell survival whereas mitochondria dysfunction is associated with loss of cellular function and viability(2,3).

In the human eye, particularly the retina, mitochondria play a central role in maintaining cellular function, with their importance most evident in the retinal pigment epithelium (RPE), a key layer of cells between the neuroretina and choroid(4). The retina, particularly the photoreceptors, has one of the highest metabolic demands in the body, requiring continuous energy to sustain visual processing(5). The majority of this energy is supplied by mitochondria, with oxygen delivered primarily through the central retinal artery (CRA) for the inner retina, while the outer retina relies on the choroidal circulation via the posterior ciliary arteries (CA)(6).

The RPE is a monolayer of highly specialized, polarized epithelial cells that serve as a crucial intermediary between the neuroretina and the choroid, forming the outer blood-retina barrier and facilitating metabolic exchange(7). Structurally, RPE cells possess apical microvilli that interact with the photoreceptor outer segments (POS), while their basal microfolds establish close contact with Bruch's membrane and the underlying choriocapillaris (5,8). Functionally, the RPE plays a vital role in maintaining retinal homeostasis through several mechanisms, including light

absorption, ion transport, phagocytosis of shed photoreceptor segments, participation in the visual cycle, and immune modulation(4,5,8). These activities are ATP-dependent, and mitochondria within the RPE serve as the primary source of this energy through oxidative phosphorylation (OXPHOS)(9–11). Dual oxygen supply by the CRA and CA, maintain an important flow of oxygen for mitochondrial OXPHOS, which in RPE cells is significantly more efficient than glycolysis alone, producing up to 16 times more ATP from glucose(5,12).

RPE cells contain an average of 700 mitochondria per cell, comprising 23.2% of the total cell volume. These mitochondria are ovoid in shape, distinct from the elongated, branching forms seen in cultured cells. Additionally, mitochondria cover 63% of the retinal imaging plane, underscoring their critical role in sustaining the high metabolic demands of the RPE(13). This high mitochondrial density ensures that RPE cells can sustain the metabolic burden associated with their protective and supportive roles. Beyond energy production, mitochondria in the RPE play a critical role in managing oxidative stress, a key factor given the retina's continuous exposure to light and high oxygen concentrations. Mitochondria are both sources and regulators of reactive oxygen species (ROS), as the electron transport chain (ETC) generates ROS as a byproduct of ATP synthesis. However, mitochondria also possess intrinsic antioxidant defenses, including superoxide dismutase and catalase, which neutralize ROS and prevent cellular damage(12,14). Maintaining this redox balance is essential, as excessive ROS can damage mitochondrial DNA (mtDNA) and proteins, potentially impairing RPE function and disrupting retinal homeostasis. Notably, during physiological conditions, mitochondrial dynamics, including fission and fusion, help preserve mitochondrial quality, ensuring that RPE cells can effectively regulate oxidative stress and sustain their essential functions such as phagocytosis and nutrient transport (5,15). Given

their role in energy metabolism and redox balance, mitochondria are indispensable for preserving the structural and functional integrity of the RPE, thereby ensuring optimal visual function.

The energy requirements provided through mitochondrial OXPHOS require a continuous oxygen supply. Disruption, inhibition or cessation of CRA and/or CA blood flow and oxygen delivery results in IRI (16–20). In the retina, this process is termed retinal ischemia-reperfusion injury (RIRI), a pathological sequence where transient ischemia, followed by reperfusion, triggers severe mitochondrial dysfunction and initiates a cascade of oxidative stress, inflammatory responses, mitochondrial apoptotic pathways(21) and retinal neurovascular degeneration(9,14,15,17,19,22,23). The retina's unique metabolic vulnerability—driven by its extraordinarily high oxygen consumption—renders it exquisitely sensitive to mitochondrial failure(10,11,19,24–26). The retinal ganglion cells (RGCs) within the inner retina have an exceptionally high metabolic demand, consuming energy at a rate comparable to or even surpassing that of the brain and heart. The brain, which accounts for only about 2% of body weight, consumes approximately 20% of the body's total energy supply. Similarly, the retina exhibits an energy demand in the same range, emphasizing its reliance on a continuous supply of oxygen and metabolites to sustain retinal neuron function(27–29). Consequently, even brief ischemic episodes can lead to irreversible neuronal loss, with complete occlusion of the central retinal artery for just 90 minutes resulting in permanent visual impairment in over 80% of patients(30–32).

During ischemia, mitochondrial respiration ceases due to lack of oxygen as the terminal electron acceptor in OXPHOS. This triggers rapid ATP depletion, loss of ion gradients, and failure of Na+/K+ ATPases, processes essential for retinal cell function and survival(22,23). In this low-energy state, cells suffer from cytotoxic edema, and progressive oxidative injury and inflammatory pathways activation(19). Upon reperfusion, reoxygenation paradoxically exacerbates damage by

triggering mitochondrial ROS production(18), driven by dysfunctional ETC complexes(17). This oxidative stress directly damages mitochondrial integrity and function. Critically, ischemia-reperfusion also primes mitochondria for death by inducing calcium overload and triggering mPTP (mitochondrial permeability transition pore) opening, which facilitates the release of cytochrome c and activates caspase-dependent apoptosis(2,21,33).

Mitochondrial dysfunction is thus not only a consequence but a primary driver of progressive neuronal loss in RIRI. Beyond acute injury, dysfunctional mitochondria also act as pathological signaling platforms, activating neuroinflammation, and disrupting inter-organelle communication(34–36). This sustained mitochondrial stress propagates secondary neurodegeneration, contributing to the long-term progression of glaucoma, diabetic retinopathy (DR), central retinal artery occlusion (CRAO), and retinopathy of prematurity (ROP)(30).

The clinical burden of RIRI is considerable, given its role in several major causes of blindness(22,23). CRAO, the acute archetype of RIRI, affects approximately 1–2 per 100,000 individuals annually, primarily older adults with vascular risk factors(37,38). Prognosis is poor(37,39), with fewer than 5% of patients regaining functional vision even with standard interventions(32). In glaucoma, chronic retinal ischemia and mitochondrial dysfunction contribute to progressive optic neuropathy, affecting over 76 million people globally, a number projected to exceed 111 million by 2040(22). Despite pressure-lowering treatments, up to 15% of glaucoma patients continue to lose significant vision over 10 years, particularly those with normal-tension glaucoma, where mitochondrial dysfunction plays a disproportionate role. Diabetic retinopathy affects over 93 million people worldwide, and expected to rise given the rising incidence in diabetes, with proliferative diabetic retinopathy (PDR) often driven by repeated cycles of retinal ischemia-reperfusion, causing progressive capillary dropout, neovascularization,

and blood-retinal barrier breakdown. Current therapies for these diseases—including anti-VEGF injections, corticosteroids, thrombolysis, hyperbaric oxygen, and laser photocoagulation—focus on managing vascular leakage, controlling inflammation, and suppressing pathological neovascularization, but they fail to restore mitochondrial function. This failure to address bioenergetic collapse is a key reason why visual outcomes remain poor, with up to 50% of patients with advanced diabetic retinopathy progressing to severe vision loss despite optimal care(12,14).

The evolving understanding of mitochondria as dynamic organelles, rather than mere bioenergetic units, has paved the way for novel therapeutic strategies that directly target mitochondrial dysfunction in human disease. Among these emerging approaches, mitochondrial transplantation (MT) has garnered particular attention as a potential paradigm-shifting intervention for conditions characterized by acute mitochondrial injury and energetic collapse.

MT refers to the isolation of functional mitochondria from healthy tissue and their direct delivery into injured tissues(40). This therapeutic strategy is grounded in the recognition that mitochondria are entities capable of facilitating metabolic support, immune modulation, and cellular rescue in times of stress(40–42).

Although intercellular mitochondrial transfer (IMT) occurs spontaneously in response to injury(11,40), therapeutic MT aims to harness and amplify this natural mechanism, providing an exogenous supply of healthy, respiration-competent mitochondria to tissues suffering from bioenergetic crisis. This concept, initially demonstrated in animal models of IRI, has now progressed to early-phase clinical investigations in pediatric cardiac surgery(43), ischemic stroke(11,16,36), and other acute conditions(16,24).

Despite this progress, the potential of MT in the context of RIRI remains unexplored and incompletely understood(11,22,24–26). Given that mitochondrial dysfunction is increasingly

recognized as the central driver of cellular injury and neurodegeneration in RIRI, targeting the retina directly with MT represents a compelling therapeutic hypothesis. Interestingly, previous studies have suggested that stem cells may rescue retinal ischemic injury by transferring functional mitochondria to damaged retinal cells through tunneling nanotubes(10,24,25). Also, recent studies indicate that delivering healthy mitochondria to the retina can protect against injury. For example, intravitreal injection of isolated mitochondria in rodent models of retinal degeneration (Royal College of Surgeons rats) attenuated retinal layer loss and preserved visual function compared to untreated controls(26). Although that model was degenerative rather than ischemic, it demonstrated feasibility as exogenous mitochondria survived in the vitreous and mitigated retinal cell loss, yet the mechanistic insights and rationale as well as dosage was not fully understood. In RIRI-specific models, direct evidence of mitochondrial transplantation is still emerging.

Mitochondrial transfer mechanism supports the biological rationale for direct MT as a therapeutic strategy in RIRI. Furthermore, beyond its immediate therapeutic potential, MT offers a unique experimental platform to dissect the molecular pathways, cellular receptors, and intracellular trafficking mechanisms that govern mitochondrial uptake and integration, opening a new avenue for research into mitochondrial biology in the context of retinal injury. This study aims to evaluate the ARPE-19 model for mitochondrial isolation, transplantation, and functional integration. Specifically, we seek to investigate mitochondrial uptake, dose selection, and the potential for MT to rescue RIRI *in vitro*, alongside transcriptomic analysis to characterize post-transplantation cellular responses.

Methods

Cell lines and cell culture

ARPE-19 cells were obtained from American Type Culture Collection (ATCC, VA, USA) and maintained in culture using standard techniques. All experiments were conducted using mycoplasma-free cells. Cells were thawed and cultured in Dulbecco's Modified Eagle Medium (DMEM)/F12 with GlutaMAX supplemented with 10% fetal bovine serum (FBS; US origin) and 5% streptomycin/penicillin for first 7-10 passages and on experiment day 0 shifted to either:

a) MEM Control Group: Minimal Essential Medium (MEM), supplemented with 1% FBS, 5% streptomycin/penicillin, or

b) MEM-Nic Group: MEM, 1% FBS, 5% streptomycin/penicillin, 0.1 mM NEAA, 1% N2 supplement, taurine (0.25 mg/ml), hydrocortisone (20 ng/ml), triiodo-thyronin (0.013 ng/ml), and 10 mM nicotinamide, all supplements were obtained from Sigma Aldrich (St. Louis, MO).

Cell culture medium was prepared fresh on experiment day 0 and kept at 4ºC for up to 30 days. Cells were seeded at a density of 1.66 /10^5 cells/cm^2 and were cultured in 24-well plates, 100mm dish plates and Falcon well/slides as needed for follow-up experiments, all culture materials were obtained from Corning (St. Louis, MO). Cells were maintained at 37°C in a 5% CO2 atmosphere. Confluence and morphology were evaluated every 24 hours and culture medium was changed 3 times a week for 14 days.

Preparation of Solutions and Buffers

The preparation of all solutions and buffers followed standard biochemical protocols as previously described(44). A 1 M K-HEPES stock solution was prepared and adjusted to pH 7.2 using KOH. Similarly, a 0.5 M K-EGTA stock solution was adjusted to pH 8.0, and a 1 M KH_2PO_4 stock

solution was prepared without pH adjustment. Solution A (SA), consisting of 300 mM sucrose, 10 mM K-HEPES, and 1 mM K-EGTA (pH 7.2), was stored at 4 °C until use. Subtilisin A (2 mg) was weighed and stored at -20 °C for later dissolution in Solution A immediately before use.

Mitochondrial Isolation

Cells were collected using 0.025% trypsin and centrifuged at 1100G for 5 minutes, the supernatant was discarded and pellet transferred into dissociation C tubes (gentleMACS™ C Tubes, Miltenyi Biotec) containing 5 mL of SA and homogenized using a pre-set mitochondrial isolation cycle on a tissue gentle dissociator using the pre-set program "h-mitochondria". 4mg of Subtilisin A were diluted in 1mL SA, then added to the homogenate, mixed, and incubated at 4 °C for 10 minutes to facilitate tissue dissociation. The homogenate was filtered sequentially twice through 40 μm and once in 10 μm mesh filters, pre-wet with SA, to remove residual cellular debris. The resulting filtrate was centrifuged at 9,500 × g for 5 minutes at 4 °C to pellet mitochondria. The mitochondrial pellet was resuspended in 1 mL of ice-cold SA or cell culture medium for subsequent functional analysis or transplantation.

Mitochodrial Dosage Selection

To determine the optimal dose for mitochondrial uptake and functional integration into ARPE-19 cells, a series of escalating mitochondrial concentrations (10^4, 10^5, 10^6, 10^7, and 10^8 mitochondria per 10,000 cells) were assessed under normal culture conditions. Mitochondrial uptake was visualized through MitoTracker Red labeling and live-cell imaging. Functional integration of transplanted mitochondria was assessed by ATP luminescence assay.

Mitochondrial Uptake

Cells were seeded overnight at a density of 40,000 cells per well in chambered coverslips with eight individual wells and high walls designed for cell culture. The following day, the cell culture medium was removed, and the cells were labeled with MitoTracker Green and DAPI according to the manufacturer's protocols to visualize mitochondria and nuclei, respectively. Freshly isolated mitochondria were labeled with MitoTracker Red immediately prior to use. Mitochondrial dosages were calculated at 1×10^{4} to 1×10^{8} per 10,000 cells and administered according to cell density. Given that 40,000 cells were seeded to ensure confluency, a 4×10^{x} dosage was used, as sub-confluent ARPE-19 cells have been shown to exhibit altered functionality(45). The labeled mitochondria were then transferred to the wells, and co-incubation was carried out for 1 hour. After co-incubation, the wells were washed to remove unincorporated mitochondria, and the cells were replenished with fresh culture medium. Live-cell imaging was performed using a confocal microscope at 40 and 65× magnification.

ATP Luminescence Assay

Mitochondrial functional integration and metabolic activity in ARPE-19 cells was assessed using an ATP luminescence assay kit according to the manufacturer's instructions (ATPlite Luminescence Assay System 96-well, Revvity, USA.). Briefly, a 10 mM ATP stock solution was prepared and diluted to create standards of varying concentrations (0.1 mM to 0.0001 mM). Cells transplanted or isolated mitochondria were plated in triplicate in a white, clear-bottom, 96-well plate along with ATP standards and a negative control (RB or cell medium). A mammalian cell lysis solution was added to all wells, and the plate was incubated at 37 °C on an orbital shaker at 125 rpm for 5 minutes. Following the addition of a reconstituted substrate solution, the plate was further incubated under the same conditions for another 5 minutes. Luminescence readings were

obtained using a spectrophotometer configured for endpoint detection. The ATP concentration in each sample was calculated based on the luminescence output and normalized using the standards, with higher readings indicating greater mitochondrial activity/ATP production.

Oxidative Stress Simulation

Cells were seeded overnight in a white, clear-bottom, 96-well plate at a density of 50,000 cells per well (following a seeding density of $1.66x10^5$cells/ cm^2). Hydrogen peroxide (H_2O_2) stock solutions were prepared in DMEM/F12 culture medium at varying concentrations (0.1 mM, 0.25 mM, 0.5 mM, 0.75 mM, and 1 mM). The medium in each well was replaced with 100 µL of either control medium or one of the prepared H_2O_2 stock solutions, with each condition plated in triplicate. Two identical plates were prepared: one underwent oxidative stress exposure for 1 hour, and the other for 4 hours. Following exposure for 1 and 4 hours, the wells were washed once with fresh room temperature medium and subsequently treated with isolated mitochondria at a dose of 1×10^6 /10,000 cells, per well, diluted in 50 µL of medium. Cell control wells received 50 µL medium only. In both groups, coincubation was performed for 1 hour. ATP levels were then quantified using an ATP luminescence assay as described. The results were used to assess mitochondrial efficacy in rescuing cellular metabolic activity under oxidative stress conditions.

Live/Dead Cell Assay Under Oxidative Stress

To evaluate the viability of ARPE-19 cells under oxidative stress and the potential protective effects of mitochondrial transplantation, a Live/Dead Cell Assay (LIVE/DEAD™ Cell Imaging Kit, Thermo Fisher Scientific) was performed following oxidative stress induction. ARPE-19 cells were seeded in 96-well plates at a density of 50,000 cells per well and allowed to adhere overnight under standard culture conditions (37°C, 5% CO_2). Oxidative stress was induced using hydrogen

peroxide (H_2O_2) at two concentrations (0.5 mM and 0.75 mM) to simulate moderate to severe oxidative damage. Cells were exposed to H_2O_2 for 1 hour, after which mitochondrial transplantation (1×10^6 mitochondria/10,000 cells) was performed in the treatment group. Control wells included cells treated with H_2O_2 but without mitochondria and untreated cells for baseline comparison.

Following 1 and 4 hours of oxidative stress and mitochondrial transplantation, the Live/Dead Cell Assay was performed using commercially available reagents that include Calcein AM (C) and Ethidium Homodimer-1 (E). Calcein AM penetrates live cells and fluoresces green upon conversion to calcein by intracellular esterases, indicating intact cell membranes. Ethidium Homodimer-1 fluoresces red when bound to nucleic acids in cells with compromised membranes, marking dead cells.

Cells were incubated with a staining solution containing 2 μM Calcein AM and 4 μM Ethidium Homodimer-1 in PBS for 30 minutes at 37°C, protected from light. Fluorescence images were captured using a fluorescence microscope at 40× magnification. Green fluorescence (live cells) and red fluorescence (dead cells) were quantified using automated image analysis software (ImageJ, Fiji). Cell viability was calculated as the percentage of live cells relative to the total cell population (live + dead). Fluorescence intensities for Calcein AM and Ethidium Homodimer-1 were analyzed using the imaging software to quantify the total number of green and red fluorescent cells. Three random fields of view per well were analyzed, and each condition was performed in biological triplicates.

Particle Size and Yield Analysis

Mitochondrial particle size and yield were determined using a particle counter (Beckman Liquid Coulter Counter, USA). Prior to measurement, the particle counter buffer was read as a blank to

ensure baseline accuracy. Following isolation, 10 µL of mitochondria resuspended in Solution A was added to the buffer of the Liquid Particle Counter for analysis. The instrument provided a measurement of particle count per milliliter, which was then multiplied by the total volume to calculate the final yield and further adjusted and titrated according to the experiment design.

RNA Sequencing

To investigate the transcriptional response of ARPE-19 cells to MT under oxidative stress mimicking RIRI, bulk RNA sequencing (RNA-seq) was performed. After previous H_2O_2 concentration analysis (0.1-1mM) ARPE-19 cells were subjected to 0.3 mM H_2O_2 for 1 and 4 hours, a concentration identified to induce sublethal oxidative stress, mimicking an environment where cells could still be rescued. Immediately following the stress period, cells were treated with freshly isolated mitochondria (1×10^6 mitochondria/10,000 cells) or left untreated as stressed controls. In parallel, a group of unstressed control cells (no H_2O_2, no MT) was included. This experimental design enabled the identification of MT-sensitive genes, those whose expression was selectively modulated by MT specifically in the context of oxidative injury, while also providing insight into how MT influences the transcriptomic landscape relative to both stressed and unstressed conditions.

After treatment, total RNA was extracted using TRIzol reagent (Thermo Fisher Scientific) following the manufacturer's protocol. Briefly, culture medium was removed, and cells were lysed directly in the culture wells with 1 mL of TRIzol reagent per well. The lysates were transferred to 1.5 mL RNase-free Eppendorf tubes, and phase separation was performed by adding 200 µL of chloroform, followed by vigorous shaking and centrifugation at 12,000 × g for 15 minutes at 4°C. The aqueous phase containing RNA was carefully transferred to a new tube, and RNA was precipitated by adding 500 µL of isopropanol and centrifuging at 12,000 × g for 10 minutes at 4°C.

The resulting RNA pellet was washed with 75% ethanol, air-dried, and resuspended in RNase-free water.

RNA concentration and purity were measured using a NanoDrop spectrophotometer (Thermo Fisher Scientific), and RNA integrity was assessed using an Agilent 2100 Bioanalyzer (Agilent Technologies). Only samples with an RNA integrity number (RIN) greater than 8.0 were used for sequencing. Library preparation was carried out using the NEBNext Ultra II RNA Library Prep Kit (New England Biolabs), following the manufacturer's instructions. Poly-A mRNA was enriched using magnetic oligo(dT) beads, and the enriched RNA was fragmented and reverse-transcribed into cDNA. Adapter ligation and PCR amplification were performed to complete the library construction. The prepared libraries were quantified using Qubit (Thermo Fisher Scientific), and size distribution was assessed with the Agilent Bioanalyzer. Libraries were pooled and sequenced on the Illumina NovaSeq 6000 platform to generate 150 bp paired-end reads.

Raw sequencing data underwent quality control using FastQC, and adapter sequences and low-quality reads were trimmed using Trimmomatic. Clean reads were aligned to the human reference genome (GRCh38) using STAR aligner, and gene expression quantification was performed with featureCounts. Differential gene expression analysis was conducted using DESeq2, with an adjusted p-value (FDR) threshold of <0.05 to determine significant changes. Following differential expression analysis, DEGs were further analyzed for temporal expression patterns to identify MT-sensitive genes — those whose expression was specifically modulated by MT at each time point. These MT-sensitive genes were subsequently subjected to pathway enrichment analysis using KEGG to elucidate how MT transcriptionally mediated a therapeutic-like effect under oxidative stress conditions. Gene ontology (GO) analysis and additional pathway enrichment were also

performed using DAVID and GSEA to comprehensively profile biological processes affected by mitochondrial transplantation.

All RNA-seq experiments were performed in biological triplicates of approximately 1 million cells for each condition (control and mitochondrial-treated) to ensure reproducibility and statistical robustness.

Statistical Analysis

Statistical analysis was conducted using R Studio. t-tests were used to compare interventions within the same group, while one and two-way ANOVA was applied for comparisons across multiple groups and interventions in selected timepoints. Data was assessed for normality and homogeneity of variance before analysis. Results are presented as mean ± standard error (SE), with statistical significance set at $p < 0.05$. For bulk RNA sequencing analysis, differentially expressed genes were identified using a fold change threshold > 1.5 and a significance level of $p < 0.05$, with false discovery rate (FDR) correction applied to control for multiple comparisons. Normalization and differential expression analysis were performed using DESeq2 in R Studio, with batch effect adjustments where necessary. Data quality control included principal component analysis (PCA) to assess sample clustering and variance stabilization. Gene ontology (GO) and pathway enrichment analyses were conducted to interpret biological significance.

Results

ARPE-19 Maturation

Under optimized *in vitro* culture conditions that included MEM supplemented with nicotinamide, N1 supplement, taurine, triiodothyronine (T3), hydrocortisone, and 1% fetal bovine serum, ARPE-19 cells demonstrated a progressive transformation over 15 days **(Figure 1)**. The cells transitioned from an undifferentiated state to a cobblestone monolayer morphology, a hallmark of mature RPE cells.

Mitochondrial Isolation

Mitochondria were isolated from ARPE-19 cells. Particle size and yield analysis revealed a sharp peak in particle size at 0.6–1.0 μm, consistent with the expected size of isolated mitochondria **(Figure 2).** The range of the size distribution was identified with a 95% confidence interval of 0.798–0.829 μm, indicating the central tendency of the particle sizes. Additionally, 90% of particles fell below 1.033 μm (d90 = 1.033 μm), with a marked decline in frequency at larger diameters, suggesting successful elimination of cellular debris and organelles exceeding mitochondrial dimensions. The particle size distribution was modeled as log-normal, with a median size (d50) of 0.711 μm and an estimated standard deviation of 0.211 μm, reflecting some spread in mitochondrial sizes. Minimal residual particles were detected beyond 2 μm, further confirming the purity of the mitochondrial fraction.

The yield assessment confirmed that a starting population of 10 million ARPE-19 cells produced approximately 1×10^9 mitochondria, demonstrating an efficient recovery process. This result was consistent across triplicate experiments, with slight variations attributable to cell culture conditions and passage number.

Isolated Mitochondria Metabolic Competence

The functional integrity of isolated mitochondria was assessed over time using ATP luminescence as a surrogate for metabolic activity. Isolated mitochondria were incubated in both cell culture medium and isolation buffer, and ATP concentrations were measured at multiple time points: 0, 30, 60, 120, and 180 minutes.

At baseline (0 minutes), mitochondria in both conditions exhibited similar ATP levels (~6.1 μM in cell culture medium and ~5.8 μM in isolation buffer), confirming comparable initial viability post-isolation. By 60 minutes, ATP concentrations declined in both conditions, with mitochondria in Solution A (SA) maintaining slightly higher ATP levels relative to cell culture medium (4.2 μM vs. 4.1 μM, respectively; mean difference = -0.12, $p = 0.99$). This trend persisted over the 2-hour period, where ATP concentrations in SA stabilized at ~4.0 μM, while mitochondria in cell culture medium displayed a more pronounced decline, reaching ~2.6 μM at 120 minutes (mean difference = -1.32, $p = 0.3274$). At 180 minutes, ATP production in both conditions was markedly reduced, with mitochondria in SA retaining slightly higher ATP levels (2.1 μM) compared to those in cell culture medium (1.9 μM, mean difference = -0.26, $p = 0.99$).

Optimal Mitochondrial Dose for Uptake and Functional Integration

ATP luminescence measurements aiming to demonstrate functional integration of mitochondria showed ATP levels of 32.0 ± 1.5 μM per 40,000 cells for 10^4 mitochondria; 33.5 ± 1.8 μM for 10^5 mitochondria; 35.0 ± 2.0 μM for 10^6 mitochondria; 30.0 ± 1.3 μM for 10^7 mitochondria; and 15.0 ± 1.0 μM for 10^8 mitochondria **(Figure 4 A)**. A significant increase in ATP/ 40,000 cells was observed at 10^6 mitochondria compared to control ($p < 0.001$). Higher doses of mitochondria

resulted in a decline in ATP levels, with 10^8 being significantly lower when compared to control ($p < 0.0001$). Doses of 10^4, 10^5 and 10^7 were no different from control ($p>0.05$) (**Figure 4 A)**. Extracellular mitochondria uptake is shown in **Figure 4 B**. Mitochondria were found to be localized within the cytoplasm in the peri nuclear area**.**

These findings indicated that 4×10^6 mitochondria per 40,000 cells was the optimal dose for maximizing uptake and functional integration into ARPE-19 cells **(Figure 4A, B)**.

Confirmation of Mitochondrial Uptake into ARPE-19 cells Using Imaging and Z-Stack Analysis

Fluorescent imaging revealed significant colocalization of red-labeled transplanted mitochondria with the green-labeled endogenous mitochondrial network, indicating successful internalization of transplanted mitochondria.

At 65x magnification, imaging demonstrated transplanted mitochondria were located within ARPE-19 cells. A clear overlap of transplanted (pink) **(Figure 5 A, D)** and host (green) **(Figure 5 B, E)** mitochondria, as shown by merged fluorescence channels, further supporting the intracellular perinuclear localization **(Figure 5C,F)**. The presence of dual-labeled mitochondria, indicated by yellow regions in the merged images **(Figure 5C, F),** could suggest physical interaction and potential fusion between transplanted and host mitochondria.

To confirm the spatial positioning of transplanted mitochondria, Z-stack imaging and three-dimensional (3D) reconstructions were performed. The Z-stack analysis validated that transplanted mitochondria were not superficial but were located within the cytoplasmic space of ARPE-19 cells.

(Figure 6). The 3D reconstructions provided an additional level of detail, illustrating the depth and true integration of transplanted mitochondria into ARPE-19 cells. Transplanted mitochondria were not observed outside of the cells or on the cell membranes.

In Vitro Oxidative Stress Model

ATP levels in ARPE-19 cells declined in a dose- and time-dependent manner following H_2O_2 exposure (Figure 7). After 1 hour, ATP remained stable at 0.1 mM (34.5 ± 2.5 μM) compared to control (36.5 ± 2.5 μM), and was modestly reduced at 0.25 mM (28.5 ± 2.0 μM, $p < 0.05$). At 0.5 mM, ATP dropped by nearly 50% (18.5 ± 2.5 μM, $p < 0.0001$), and levels were nearly undetectable at 0.75 mM (3.0 ± 0.8 μM) and 1 mM (2.0 ± 0.5 μM) **(Figure 7 A)**. After 4 hours, ATP remained preserved at 0.1 mM (53.0 ± 3.0 μM) and 0.25 mM (51.0 ± 2.5 μM), but declined significantly at 0.5 mM (38.0 ± 3.0 μM) and was almost completely depleted at 0.75 mM (2.5 ± 0.6 μM) and 1 mM (0.5 ± 0.2 μM) ($p < 0.0001$) **(Figure 7 B)**. These results confirm that H_2O_2 induces a concentration- and time-dependent loss of cellular energy, validating this model for oxidative stress induction.

Mitochondrial Rescue of Oxidative Stress After 1 Hour

At 0.1 mM H_2O_2, MT restored ATP levels to approximately 42 μM/50,000 cells, representing a 5% increase compared to untreated stressed cells (approximately 40 μM), though this difference was not statistically significant (ns). MT improved ATP production compared to untreated controls after 1 hour of stress at 0.25mM H_2O_2 concentrations **(Figure 8-A)** significantly elevating ATP levels to approximately 50 μM/50,000 cells, representing a 36% increase, compared to untreated stressed cells (approximately 37 μM, $p < 0.0001$), fully restoring ATP production to levels above

the unstressed control baseline. At 0.5 mM H_2O_2, ATP levels reached approximately 22 µM/50,000 cells in transplanted cells, a slight increase compared to untreated stressed cells (approximately 20 µM), but this effect was not statistically significant (ns). At higher H_2O_2 concentrations of 0.75 and 1 mM, MT failed to restore ATP production, with both treated and untreated cells showing ATP levels near zero **(Figure 8-A).**

Mitochondrial Rescue of Oxidative Stress After 4 Hours

After 4 hours of stress, MT significantly improved ATP production compared to untreated controls at 0.1 - 0.5mM H_2O_2 concentrations **(Figure 8-B)**. At 0.1 mM H_2O_2, MT restored ATP levels to approximately 54 µM/50,000 cells, representing a 12.5% increase compared to untreated stressed cells (48 µM, $p < 0.01$), fully restoring ATP to levels slightly exceeding the baseline seen in unstressed controls (52 µM). At 0.25 mM H_2O_2, MT restored ATP levels to approximately 54 µM, representing a 15% increase compared to untreated stressed cells (47 µM, $p < 0.01$), again achieving full recovery to baseline. At 0.5 mM H_2O_2, ATP levels in transplanted cells reached approximately 50 µM, representing a 43% increase compared to untreated stressed cells (which retained only ~35 µM ATP, $p < 0.001$). However, at 0.75 mM and 1 mM H_2O_2, MT failed to restore ATP production, with ATP levels dropping to below 6 µM and near zero, respectively, and no significant differences were observed between treated and untreated groups (ns) **(Figure 8-B).**

Mitochondrial Rescue of Oxidative Stress After 1 and Hours with 0.3mM H_2O_2

At 0.3mM concentration H_2O_2, ATP levels measured after 1-hour stress and 1-hour MT, showed reductions under oxidative stress, with values decreasing to 36.69 – 47.81 mM, representing a 12–25% decline compared to the mitochondrial-treated group ($p = 0.0342$). In contrast, cells receiving mitochondrial treatment exhibited higher ATP levels, ranging from 39.31 to 52.21 mM, indicating

partial preservation of energy metabolism. After 4 hours of oxidative stress, ATP depletion in untreated cells had values declining to 31.45–39.49 mM, corresponding to a 23–47% reduction relative to mitochondrial-treated cells ($p < 0.001$). MT mitigated this loss, maintaining ATP levels between 49.76 and 59.28 mM. .

Collectively, these findings demonstrate that MT rescues ATP production under at 0.25mM H_2O_2 after 1-hour and 0.1 - 0.5mM H_2O_2 concentrations after 4-hours **(Figures 7-8).**

Live/Dead Cell Assay

MT appears to mitigate oxidative stress-induced cell death in ARPE-19 cells. Live/Dead staining revealed a dose-dependent increase in cell death with concentrations of H_2O_2 from 0.1 mM to 1 mM, as evidenced by increased red fluorescence (Ethidium Homodimer-1 positive cells) across conditions (**Figure 9-A)**. Control cells exhibited predominantly green fluorescence (Calcein AM positive), while H_2O_2 concentrations ≥ 0.75 mM resulted in a notable increase in red fluorescence.

Quantitative analysis of EthD-1 positive cells showed a significant rise in cell death with increasing H_2O_2 concentrations. In the absence of mitochondrial treatment, EthD-1+ cells increased progressively, reaching approximately 25% at 0.5 mM and over 25% at .75 mM H_2O_2. However, MT significantly reduced the percentage of EthD-1+ cells, specially, mitochondrial treatment decreased cell death at 0.25 mM, 0.5 mM, and 0.75 mM H_2O_2 concentrations by approximately 40% compared to untreated controls (**Figure 9-B).**

RNA Sequencing Analysis

In both the 1-hour and 4-hour stress conditions, distinct expression patterns of differentially expressed genes (DEGs) are observed across the experimental groups. The heatmap visualization

highlights differences in gene expression profiles between Vehicle-treated and MT cells at both time points, illustrating variation in transcriptomic responses after oxidative stress conditions **(Figure 10)**.

Data quality was assessed using PCA. The PCA plot illustrates the distribution of transcriptomic profiles, with Vehicle-treated and MT samples displaying distinct clustering patterns along the principal components **(Figure 11).** The volcano plots illustrate the differential gene expression analysis between Vehicle-treated and MT cells at 1 and 4hours **(Figure 12).** Genes with significant changes (log_2 fold change > 1.5, $p < 0.05$) are highlighted, showing distinct upregulated and downregulated genes in response to MT.

At the 1-hour post-transplantation timepoint, Gene Ontology (GO) enrichment analysis of differentially expressed genes revealed strong over-representation of processes related to nuclear division, chromosome segregation, nucleosome assembly, and organelle fission **(Figure 13).**

Further analysis through clustered gene expression profiling identified mitochondria-sensitive genes, revealing distinct expression patterns. Notably, MT groups exhibited profiles more similar to unstressed controls compared to vehicle-treated groups at 1-hour group **(Figure 14)**. To further illustrate this shift, a heatmap of these MT-sensitive DEGs at 1 hour was generated, providing a visual representation of gene expression changes across conditions **(Figure 15).** Using these gene sets, we proceeded with KEGG pathway enrichment analysis to explore the associated biological processes and pathways.

KEGG pathway enrichment analysis of these MT-sensitive genes at 1-hour post-transplantation highlighted downregulation of apoptosis, inflammation, and pathological angiogenesis (Figure

16). Apoptotic signaling was associated with downregulation of CASP9, a key initiator of mitochondrial apoptosis. Inflammatory signaling showed reduced expression of FOSB in the IL-17 pathway, alongside downregulation of cGMP-PKG signaling, T cell receptor signaling, B cell receptor signaling, IL-6 and IL-6R signaling pathways, and differentiation pathways for Th1, Th2, and Th17 cells. VEGF signaling and PD-L1 checkpoint signaling, key drivers of stress-induced angiogenesis and inflammation, were also downregulated.

Post-transplantation, in cells that had undergone 4 hours of oxidative stress, GO enrichment revealed enrichment in processes related to mitochondrial membrane permeability regulation, myofibril assembly, glutathione biosynthesis, and cellular responses to external stimuli **(Figure 17).** Further analysis of clustered gene expression at the 4-hour time point identified MT-sensitive genes with distinct transcriptional patterns **(Figure 18).** Notably, MT-treated groups exhibited expression profiles that more closely resembled unstressed controls compared to vehicle-treated groups as well as unique differential patterns, suggesting additional enrichment of genes not related to unstressed controls **(Figure 19).** To better visualize this shift, a heatmap of these mitochondria-sensitive DEGs was constructed, highlighting gene expression differences across conditions. KEGG analysis of MT-sensitive genes at 4 hours revealed upregulation of anti-inflammatory genes within TNF signaling and NF-kappa B signaling, suggesting a fine-tuned anti-inflammatory response **(Figure 20).** Additionally, immune signaling pathways such as PD-L1 checkpoint, T cell receptor signaling, B cell receptor signaling, and Th differentiation pathways were partially re-engaged, with upregulation of genes within their pathways.

MT also induced upregulation of genes within the MAPK signaling cascade, including DUSP5, DUSP6, RASA2, NR4A1, and FOS, suggesting possible stress-adaptive

kinases known to promote survival. TGF-beta signaling, via upregulation of INHBA and BMP2, supported extracellular matrix remodeling, consistent with enhanced structural recovery. Interestingly, cyclic nucleotide signaling (cAMP and cGMP-PKG pathways) remained upregulated, suggesting sustained metabolic and cytoskeletal adaptation.

Discussion

In this study we sought to establish and optimize a reliable cell line capable of recapitulating the critical functions of the RPE, a vital component of the retina that provides structural support, nutrient transport, and essential metabolites for the visual cycle. Native RPE cells play a crucial role in maintaining the retinal blood barrier (BRB), photoreceptor function, and overall retinal health. However, the direct use of primary RPE cells presents significant challenges, including the difficulty in obtaining human donor eyes, physiological variability, limited availability, and the time-intensive purification process that often yields suboptimal cell populations. Additionally, mortal cell lines exhibit restricted passage numbers, reducing their utility for extended experimental workflows.

Given these limitations, we sought to establish an alternative protocol using the widely available ARPE-19 cell line. This immortalized human RPE cell line is advantageous due to its reproducibility, scalability, and cost-effectiveness. However, ARPE-19 cells often lack the mature epithelial phenotype observed in native RPE cells, requiring specific culture conditions to induce proper differentiation and regain functionality. To address these challenges, we adopted the ARPE-19 cell line, a well-established immortalized human RPE model, and implemented a targeted differentiation protocol(46) to induce a mature, epithelial-like phenotype. The maturation of ARPE-19 cells into a cobblestone monolayer closely resembling native RPE, allowed us to create a scalable, reproducible platform capable of modeling RIRI-relevant oxidative stress responses, However, to strengthen the translational value of our findings, future studies could incorporate a tiered validation strategy. Induced pluripotent stem cell (iPSC)-derived RPE cells provide a human-relevant platform with improved fidelity in gene expression and polarity, though maturity must be carefully confirmed. Retinal organoids generated from human pluripotent stem cells

present a three-dimensional tissue-like environment to assess cell-cell interactions and layered retinal architecture. For in vivo validation, animal models, especially rodents subjected to transient retinal artery occlusion to mimic RIRI could offer insights into systemic and immunologic effects of MT. When feasible, non-human primates may serve as an intermediate step to bridge preclinical and clinical applications. Each model offers unique advantages depending on the endpoint: iPSC-derived cells for mechanistic studies, organoids for structural validation, and animal models for systemic translation.

In our system, isolated mitochondria retained metabolic competence post-isolation, as shown by functional ATP production for at least one hour when suspended in DMEM/F12 supplemented with 10% FBS ensuring that transplantation occurred during a defined viability window **(Figure 3).** It has been suggested that isolated mitochondria cannot survive calcium overload during transplantation(47). However, our experiments and previous studies(16,40,43,44,48) directly challenge this assumption. In our system, isolated mitochondria maintained functional ATP production for at least one hour when suspended in DMEM/F12 supplemented with 10% FBS, a medium containing approximately 1.7 mM calcium, a concentration that reflects the typical extracellular environment in culture. No statistical difference was shown when compared to maintenance in Solution A in any timepoint ($p>0.05$) **(Figure 3)**. Despite this calcium exposure, mitochondria were successfully internalized by ARPE-19 cells, as confirmed by live imaging and Z-stack colocalization, demonstrating not only survival but also functional integration into the host mitochondrial network **(Figures 4, 5, 6, 8**). This highlights the importance of context, suggesting that mitochondria can tolerate physiologic calcium loads during therapeutic transplantation if performed within appropriate time windows.

Functional Integration and Bioenergetic Rescue

We determined dosing based on particle number (x mitochondria per 10,000 cells), following precedent from cardiac, oncological and skeletal muscle models(49,50). This metric is practical and allows for controlled, reproducible transplantation across experiments. However, it does not account for functional variability or potential heterogeneity in mitochondrial integrity. Our particle size analysis showed a predominant peak at 0.6–1.0 μm, consistent with the expected size range. We did not fractionate mitochondria based on size, opting instead to use the full mitochondrial population. While mitochondrial size has not traditionally been used to stratify function, emerging evidence from neuronal models(51) suggests smaller mitochondria may support synaptic activity, indicating potential specialization. Investigating size-dependent effects was beyond our scope but may be a valuable future direction to refine functional transplantation strategies.

To ensure consistency across mitochondrial isolations, we standardized key parameters: the number of starting ARPE-19 cells, passage number, isolation buffers, and processing conditions. Particle size and count were routinely measured to verify uniformity.

At an optimized transplantation dose of 1×10^6 mitochondria per every 10,000 cells, mitochondrial uptake was confirmed by live-cell imaging, colocalization within the host cell, and Z-stack 3D reconstructions. The identification of 1×10^6 mitochondria per 10,000 cells as the optimal dose for ARPE-19 cells fits within the established dose-response relationship observed in previous cardiac and neuronal ischemia models(43,52). This supports the notion that effective MT requires careful titration to match cellular uptake capacity, which will likely vary between tissues and disease states(16,43,52). This functional integration produced a clear dose-dependent ATP rescue, strongly indicating that transplanted mitochondria directly contribute to host bioenergetics.

Moreover, identifying a precise mito-to-cell ratio, 100:1, this pattern suggests a physiological threshold in which MT may be ineffective or even detrimental.

Several mechanisms may explain this(53). At high concentrations, cells may experience physical overload, with excess organelles disrupting intracellular architecture or occupying space needed for normal trafficking and signaling. A large influx of mitochondria may also shift ionic homeostasis as each organelle carries membrane potential and ionic gradients, and introducing too many could alter intracellular calcium or potassium levels, interfering with native signaling or triggering stress responses. In addition, mitochondria possess a strong negative membrane potential(54); excessive accumulation near the cell surface could repel the cell's own membrane or alter local electrochemical gradients, possibly hindering uptake. High external mitochondrial concentrations may also increase medium viscosity or promote aggregation, limiting their internalization and creating extracellular debris that could compromise the culture environment. In this case, our results represent a valuable starting point for the translational potential of MT, as it provides a foundation for dose optimization in future in vivo models and eventual clinical applications, strengthening the impact of this research. Taking into account that the human eye has approximately 3–4 million RPE cells(55), the dosage would likely be around 3×10^8, which correlates with previous study dosages(16,43,49) and remains within the feasible range for mitochondrial isolation, making it a possible translatable model, strengthening these findings.

Collectively, these findings **(Figures 4-6)** confirm that the transplanted mitochondria are internalized, colocalize with the host mitochondrial network, and occupy a three-dimensional intracellular space, reinforcing their functional integration into ARPE-19 cells.

In our study, we used H_2O_2 as a surrogate to model oxidative stress associated with RIRI, applying a range of concentrations to simulate dose-dependent injury and assess MT efficacy. This method

enabled us to generate reproducible, quantifiable stress levels and map mitochondrial rescue effects. While H_2O_2 models oxidative stress effectively in RPE(56), it does not encompass the full pathophysiology of RIRI, which involves ischemia, metabolic depletion, reperfusion, inflammation, and fluctuating oxygen gradients. To improve the model's physiological relevance, future experiments could pair H_2O_2 exposure with glucose deprivation, mimicking metabolic crisis more accurately. Hypoxia-reoxygenation and ex vivo retinal perfusion models, while closer to in vivo ischemia, are technically challenging and less standardized. In our model, H_2O_2 effectively in a dose-dependent matter, decreased function, as shown by ATP content /cells and increased cell death **(Figures 8, 9).**

Under 1 hour of oxidative stress at 0.25 mM H_2O_2, mitochondrial transplantation restored ATP levels to approximately 50 µM/50,000 cells, fully exceeding the unstressed baseline and representing a 36% increase compared to untreated stressed cells ($p < 0.0001$). After 4 hours of oxidative stress, ATP rescue at this dose reached approximately 54 µM, with statistically significant recovery compared to untreated stressed cells ($p < 0.001$). This suggests sustained bioenergetic benefit even under prolonged stress.

At higher oxidative stress concentrations (0.5 mM H_2O_2), MT provided partial ATP recovery, reaching 22 µM after 1 hour and 50 µM after 4 hours, representing 43% rescue ($p < 0.001$). However, at ≥0.75 mM H_2O_2, ATP rescue collapsed, highlighting a clear threshold beyond which damage exceeds mitochondrial rescue capacity. This threshold aligns with known irreversible oxidative injury thresholds for RPE and cardiac myocytes(22,52).

MT also significantly reduced cell death, particularly at 0.25 mM and 0.5 mM H_2O_2, where EthD-1+ cells (indicating membrane rupture) decreased compared to untreated stressed cells ($p < 0.001$).

This cytoprotective effect persisted even at 4 hours of stress, demonstrating that MT might not merely delay cell death but indicates a possible suppression of oxidative injury progression. This protective profile strongly resembles data from myocardial and cerebral ischemia models(57–59). These results indicate that MT effectively reduces oxidative stress-induced cell death in ARPE-19 cells, suggesting its potential as a therapeutic intervention for oxidative damage.

While vehicle-treated cells served as our controls, they do not control for potential non-specific effects of exogenous mitochondrial material, therefore we acknowledge that future experiments should incorporate non-functional mitochondria, such as heat-inactivated or depolarized organelles, to distinguish between functional rescue and passive effects of uptake or mitochondrial components. Including such controls would also help elucidate whether immunogenicity or metabolic signaling contributes to observed rescue effects.

Following the dose-dependent analysis, we selected 0.3 mM H_2O_2 as the optimal concentration for subsequent experiments, as it induced a level of injury resembling ischemia rather than apoptosis. The objective was to establish a condition where cellular damage was sufficient to evaluate MT efficacy without exceeding a threshold that would render rescue ineffective.

Altogether these effects demonstrate that MT might be a therapeutic alternative when cellular and mitochondrial damage remains reversible. ARPE-19 seem to show resilience to ROS-induced damage at concentrations of H_2O_2 0.1-0.5mM at 1-hour, correlating with the literature describing the RPE as a tissue with compensatory mechanisms towards ROS (23,27,55,56), however concentrations of H_2O_2 $\geq$0.75mM at 1 and 4 hours reduce the efficacy of MT, suggesting a threshold beyond which ROS-mediated damage becomes irreversible.

The efficacy of MT to rescue mitochondrial dysfunction-induced damage seem to be more apparent after 4 hours of stress show by the significant rescue at concentrations 0.1 - 0.5mM H_2O_2 **(Figure 8).** These findings align with previous research(14,27,55,57) and suggest that while ARPE-19 cells possess an inherent resistance to oxidative stress, this defense is not indefinite. Prolonged exposure, even at low concentrations of oxidative agents, leads to cumulative damage, overwhelming the cells protective mechanisms. The ability of transplanted mitochondria to integrate functionally and restore ATP production underscores their potential as a therapeutic approach for oxidative stress-related injuries, including ischemia-reperfusion injury.

Importantly, oxidative stress damage pattern closely mirrors documented ischemia-reperfusion across multiple tissues(17,18,59,63,64).

Transcriptomic Remodeling

To further assess the impact of MT on the transcriptomic landscape of ARPE-19 cells subjected to oxidative stress, bulk RNA sequencing was performed following 1 and 4 hours of oxidative stress with 0.3 mM H_2O_2. This concentration was selected to induce oxidative stress without causing extensive cell death, allowing for the evaluation of early transcriptional responses. MT was carried out immediately after oxidative stress exposure for either 1 or 4 hours to investigate its potential in modulating gene expression related to stress response, metabolic adaptation, and cellular recovery.

To dissect the transcriptional impact of MT in greater detail, we first performed DEG analysis to identify individual genes significantly altered by MT under oxidative stress conditions **(Figures 10-13).** However, to gain a more systems-level understanding, we then conducted clustered

analysis to group genes into clusters based on their expression patterns over time **(Figures 14, 15, 18, 19**). This allowed us to pinpoint MT-sensitive gene clusters, identifying which coordinated gene sets were most responsible for shifting the transcriptomic profile closer to that of unstressed, healthy cells. This two-step approach, moving from broad DEG identification to targeted cluster analysis, suggested a clearer therapeutic-like signature, helping us determine which transcriptional programs were most actively engaged in the reparative and protective effects conferred by MT.

General DEG revealed transcriptional remodeling induced by MT at both time points — after 1 hour of MT following either 1 hour or 4 hours of oxidative stress. This reflects both rapid and evolving transcriptional responses to MT across early and prolonged stress conditions. Volcano plots highlighted significantly up- and downregulated genes in MT-treated cells compared to untreated stressed controls, with early transcriptional responses centered on cellular stress defenses, mitochondrial function, and survival pathways **(Figure 11).** Principal Component Analysis (PCA) demonstrated separation between mitochondrial-treated and untreated groups, suggesting the possible impact of MT on global gene expression **(Figure 10).** However, we also observed some variance within groups. Understanding the sources of this variance is important for data interpretation and for designing future studies to minimize unwanted variability. Biological variation is one contributor. Even though ARPE-19 is a clonal cell line, subtle differences between replicates (cell density, cell cycle stage, or innate heterogeneity in differentiation state) can cause gene expression differences. For instance, one replicate might have had a slightly higher cell density at time of treatment, influencing its transcriptome (confluent ARPE-19 tend to express some RPE genes more strongly(45)). Similarly, biological noise in oxidative stress induction due to technical performance can lead to variance in stress-responsive gene expression. Such biological and technical noise often shows up in PCA as dispersion within what is nominally the same group.

A general heatmap of the differentially expressed genes further illustrated distinct patterns of MT-treated cells **(Figure 9).** DEGs were further clustered into distinct temporal expression patterns, identifying gene clusters whose expression was specifically modulated by MT (MT-sensitive genes). Hierarchical clustering of DEGs confirmed distinct separation between groups, with MT-treated cells clustering away from untreated stressed cells and closer to unstressed controls, consistent with early transcriptional rescue **(Figures 14, 18)**.

RNA sequencing suggested that MT triggered a transcriptomic remodeling, shifting stressed cells toward a gene expression profile closer to unstressed controls. This occurred within 1 hour and persisted after 4 hours, adding to the hypothesis that functional mitochondrial integration immediately triggers stress adaptation. This is a particularly relevant finding given that transcriptional plasticity, the ability of cells to rapidly reprogram gene expression under stress, has been recognized as a critical determinant of survival in ischemic tissues(65).

At the 1-hour timepoint, key pathways **(Figure 16)** related to apoptosis, IL-17 inflammatory signaling, VEGF signaling, cGMP-PKG signaling, T cell and B cell receptor signaling, and Th1, Th2 and Th17 cell differentiation were all downregulated. This observation further aligns with where mitochondrial disfunction amplifies IL-17 and VEGF pathways, contributing to secondary injury and pathological immune response(21,66). Within these pathways, NFATC2 downregulation stood out as a central node linking inflammation, immune cell activation, and pathological angiogenesis. NFATC2 regulates inflammatory cytokine production, including IL-2 and TNF-α, while also modulating VEGF expression during stress-induced neovascularization(67,68). Its suppression suggests that MT not only might limit immediate pro-inflammatory cytokine release but also suppress pathological angiogenesis that could otherwise

worsen retinal edema and neovascular pathology(68). Together, these transcriptional changes propose a coordinated shift away from inflammatory and pro-death signaling, favoring cytoprotection and immune quiescence at 1 hour.

IL6 has been described as a mediator of mitochondrial dysfunction and age-related physical decline(69). Recently, it has been demonstrated that IL6/IL6R suppresses mitochondrial function through the gp130-JAK1/STAT1/3-HIF1α-ERRα axis, leading to impaired respiration and ATP production(70), while it has been shown showed that chronic IL6 elevation in a humanized mouse model accelerates mitochondrial dysregulation and frailty, confirming its role in systemic aging(69). Given these findings, it is particularly interesting that our study found IL6 and IL6R to be specifically downregulated following MT. This hints that MT may counteract IL6-driven mitochondrial suppression by disrupting the inflammatory signaling cascade responsible for impairing mitochondrial function. One possible explanation is that MT restores mitochondrial function, thereby reducing IL6-mediated activation of HIF1α and preserving ERRα activity. Alternatively, the transplanted mitochondria could be modulating immune responses, directly suppressing IL6 production and its downstream effects. This raises the intriguing possibility that MT not only replenishes mitochondrial capacity but also proposes a reshaping of the inflammatory environment, potentially mitigating IL6-induced damage in RIRI and other conditions characterized by chronic inflammation and mitochondrial decline.

Interestingly, downregulation of cGMP-PKG signaling after MT may represent a protective mechanism as recent transcriptomic studies in degenerative retinal models have revealed that the cGMP-PKG axis also acts as a transcriptional regulator directly inhibiting oxidative phosphorylation and mitochondrial biogenesis programs(71). In models of retinitis pigmentosa

(RP), sustained activation of cGMP-PKG signaling suppresses mitochondrial gene expression and accelerates photoreceptor degeneration. Conversely, inhibition of PKG rescues mitochondrial function and improves retinal cell survival(71). This aligns with our observation that MT downregulates cGMP-PKG signaling, advocating for the possibility of limiting signals that would otherwise aggravate post-ischemic retinal injury.

After 4 hours of stress and 1-hour post-MT, transcriptional programs **(Figure 20)** showed upregulation of TNF signaling, NF-κB signaling, TGF-beta signaling, PD-L1 expression, and efferocytosis. This suggests an immune recalibration process with early downregulation of hyperinflammatory cascades followed by targeted re-engagement of reparative immune functions. In fact, the upregulation of efferocytosis-related genes, including DUSP5 and SGK1, brings the idea that MT not only could preserve surviving cells but also actively foster the clearance of apoptotic debris, a process essential for limiting chronic inflammation and enabling constructive repair(72).

Several key regulatory nodes emerged from the transcriptomic analysis, pointing to a possible mechanistic insight into how MT reprograms cellular fate. Downregulation of CASP9 and DDIT4 directly suggest possible suppression of intrinsic apoptosis and stress-induced metabolic shutdown. The downregulation of CASP9 following MT represents modulation of the intrinsic apoptotic pathway, which is directly triggered by RIRI(11,19,22,23). CASP9 acts as the apical activator caspase, initiating the intrinsic apoptosis cascade. Its inhibition has been shown to significantly reduce apoptosis and protect neurons from IRI(21,66). DDIT4 normally acts as a sensor that couples oxidative stress to mTORC1 inhibition**,** driving cells into energy-conserving autophagy or death pathways(73–75). Its downregulation after MT highlights active metabolic

rescue rather than simple antioxidant effects. This is particularly interesting because DDIT4 activation has been linked to neurodegeneration, inflammation and stress responses(73–75).

The observed upregulation of SGK1 after MT aligns with the cytoprotective role of SGK1 in IRI across multiple organ systems, particularly in the heart(76). SGK1, a serine/threonine kinase, is a known stress-responsive regulator that integrates signals from oxidative stress, hypoxia, and ischemia, activating downstream pathways that preserve ionic balance, stabilize mitochondrial function, and suppress apoptotic cascades(76,77). In myocardial IRI, SGK1 upregulation has been shown to reduce infarct size, attenuate inflammatory responses, and improve functional recovery of ischemic tissue, effects partly mediated through its regulation of membrane channels, inflammatory cytokines, and mitochondrial membrane potentials(76). Moreover, studies in cardiac transplantation models demonstrated that dexamethasone-mediated induction of SGK1 in donor hearts reduced cardiomyocyte injury and enhanced graft survival, directly implicating SGK1 as a driver of ischemic tolerance and adaptive remodeling(78). This protective role has also been documented in renal IRI models, where SGK1 activation enhances cellular stress resilience and mitigates apoptotic death(79,80). Therefore, the significant upregulation of SGK1 observed in our transcriptomic analysis following MT strongly supports the interpretation that MT triggers a conserved pro-survival program in ARPE-19 cells, similar to the protective response seen in heart, kidney, and brain under ischemic stress.

Upregulation of DUSP5 and DUSP6, which inhibit ERK signaling, further suggests inhibition of MAPK-driven inflammatory amplification(81). This might indicate an early attempt to restore MAPK homeostasis under oxidative stress. Both phosphatases are stress-inducible regulators that selectively deactivate ERK signaling, and their increased expression has been associated

with cytoprotective and neuroprotective roles in neural cells exposed to injury(82–84). By limiting sustained ERK activation, DUSP5/6 could help prevent excessive inflammatory and apoptotic responses, processes strongly implicated in RIRI. In fact, restoration of DUSP activity has been proposed as a therapeutic strategy to counteract MAPK-driven neurotoxicity in several pathological contexts, reinforcing the idea that MT-induced DUSP upregulation may contribute to the broader stress adaptation and survival program triggered by MT in the ischemic retina(83,84).

We also observed upregulation of LDLR (low-density lipoprotein receptor) at 4 hours after MT. Recent work demonstrated that LDLR exerts critical neuroprotective effects in ischemia-reperfusion injury. Research has shown that loss of LDLR in ischemic models amplified inflammasome signaling, worsened neuronal death, and aggravated functional deficits(85).

Alongside FOS, genes such as CXCL3, TNFAIP3, JUNB, and EDN1 followed a similar pattern of delayed activation — highlighting that MT does not completely suppress inflammation but instead apparently recalibrates it toward constructive resolution and compensation. For example, the observed upregulation of TNFAIP3 following mitochondrial transplantation in ARPE-19 cells exposed to oxidative stress may have particular relevance within the context of retinal inflammation and innate immune signaling. Recent work has demonstrated that TNFAIP3 regulates retinal endothelial cell inflammatory responses by modulating the activity of toll-like receptor 4 (TLR4) and the NOD-like receptor protein 3 (NLRP3) inflammasome(67,86–88). In retinal tissue, loss of TLR4 increases TNFAIP3 levels, which in turn leads to suppression of NLRP3 inflammasome activation (86). Upregulation of TNFAIP3 may indicate that MT helps restore regulatory brakes on inflammatory cascades, potentially limiting the chronic, sterile inflammation that drives retinal degeneration after ischemia-reperfusion injury.

This transcriptional reversion towards homeostasis, coupled with downregulation of apoptosis and inflammation and enhancement of metabolic flexibility and structural repair, underscores MT's multi-dimensional mechanism of action. Rather than acting through a single pathway, MT appear to trigger a coordinated cellular response spanning mitochondrial quality control, immune regulation, metabolic recalibration, and structural resilience.

Clinical Translatability of Mitochondrial Transplantation to the Retina

Translating MT into a viable therapy for retinal diseases demands a careful orchestration of delivery strategies, donor selection, and application to disease-specific contexts. The eye, with its unique accessibility and immune-privileged compartments, offers an ideal setting to pioneer this approach, but its complexity also poses important translational challenges.

In vitro, mitochondrial delivery is straightforward; however, in vivo application requires precision. Intravitreal (IV) injection, already well established in ophthalmology, offers a practical method to introduce mitochondria into the vitreous, from which they may access inner retinal layers such as ganglion cells and Müller glia. Encouragingly, preclinical studies in models of retinal degeneration have demonstrated that mitochondria delivered IV can integrate into host cells, preserve retinal thickness, and sustain photoreceptor viability(26). This approach is minimally invasive, repeatable, and logistically similar to anti-VEGF administration, making it a strong candidate for acute conditions such as central retinal artery occlusion or traumatic optic neuropathy.

Yet, IV may be insufficient when targeting outer retinal structures like photoreceptors or the RPE, as these are anatomically distant from the vitreous interface. In such cases, subretinal injection, which places therapeutic material directly between the neural retina and RPE, may enable more

efficient uptake. Although more invasive, this method is already used in gene and cell therapies, and may be particularly suited for chronic degenerative diseases such as geographic atrophy, Stargardt or perhaps Lebers disease, where direct rescue of RPE or photoreceptor cells is needed.

A critical aspect of translation is the source of donor mitochondria. Autologous transplantation, using mitochondria derived from the patient's own skeletal muscle or mesenchymal stem cells, offers immunological compatibility and has shown efficacy in preclinical and clinical cardiac and neurologic models(49,52,57). However, the logistics of isolating and preparing autologous mitochondria limit their utility in time-sensitive scenarios(40). Alternatively, mitochondria isolated from standardized cell cultures offer an attractive solution: they could be expanded under defined, pathogen-free conditions, free from pathological haplotypes, and manufactured using codified protocols that ensure batch-to-batch consistency and high functional quality. This controlled approach could reduce variability, minimize the risk of host incompatibility, and support the development of banked, ready-to-use mitochondrial preparations suitable for allogeneic applications.

Therapeutic strategies will also differ depending on disease kinetics. In acute retinal injuries, such as ischemia-reperfusion events, a single high-dose IV injection of mitochondria before (stent-related ocular ischemic syndrome) or after (CRAO, BRAO) the event, might mitigate irreversible cell death by rapidly restoring bioenergetic function. In contrast, chronic conditions like glaucoma or dry age-related macular degeneration may require a sustained or repeated dosing approach, aimed at gradually augmenting cellular resilience and metabolic stability. For example, periodic IV injections of mitochondria could provide ongoing support to stressed retinal ganglion cells or degenerating RPE over time.

Importantly, small animal studies report no inflammatory responses to intraocular mitochondrial delivery(24,26), and some suggest anti-inflammatory effects mediated by restored mitochondrial function(10), rigorous safety evaluations in large animal models remain necessary. Assessing risks such as increased intraocular pressure, inflammatory uveitis, or retinal detachment is essential. In this context, it is worth noting that RPE cells upregulate PD-L1 and other immune-regulatory molecules under stress, a response that may further support immune tolerance of MT within the ocular environment.

Beyond therapeutic rescue, MT also provides a valuable platform for discovery. By mapping the transcriptional and signaling responses elicited by viable mitochondria in damaged retinal cells, we may uncover critical pathways, mediators, and molecular messengers involved in cellular repair and survival. This knowledge could inform the development of adjunct or alternative therapies that harness downstream effects, such as cytokine modulation, metabolic adaptation, or apoptotic control, without necessarily requiring full mitochondrial transfer. In this sense, mitochondria may serve not only as a therapeutic tool, but as a biological lens through which to identify new intervention targets.

Lastly, clinical implementation will require the development of standardized manufacturing protocols to ensure mitochondrial purity, viability, sterility, and scalability. Although this remains a technical hurdle, progress in other fields(40,41,48) demonstrates a growing feasibility of mitochondrial-based interventions. With the retina's accessibility, the urgency of unmet therapeutic needs, and the compelling early evidence of functional rescue, MT stands as a promising frontier in neuroprotective retinal therapy. Its clinical translation will rely not only on

delivery and sourcing strategies, but also on our ability to define dosing paradigms that match the temporal and cellular demands of each retinal disease.

Conclusion

Taken together, these results establish MT as promising new avenue for research as a multi-dimensional systems intervention for oxidative stress-induced injury in retinal cells. Rather than addressing isolated downstream pathways, MT suggests rescue of the bioenergetic collapse that initiates apoptosis, inflammation, and immune dysregulation in RIRI. This places MT as a valid possible target upstream of conventional anti-inflammatory or anti-angiogenic therapies, offering the potential for true disease modification. We also observed that its efficacy is inversely related to the degree of structural injury already present at the time of delivery.

In this study, we not only identified an optimal transplantation dose for ARPE-19 cells but also proposed some mechanistic insights into mitochondrial integration, stress modulation, and partial functional recovery. Furthermore, we identified molecular players that may represent interesting study targets, paving the way for future research into mitochondrial-driven treatment strategies.

Beyond its role as a bioenergetic powerhouse, mitochondria function as key regulators of cellular homeostasis, signaling, and immune modulation. Our findings highlight that MT might not act through a single mechanism but suggest some interesting hypotheses of acting across multiple pathways, in a time-dependent and multifaceted rescue process that could converge on cellular survival. This reinforces the modern proposed view of mitochondria as a holistic, systems-wide organelle with the potential to influence cellular fate through diverse molecular and metabolic networks. It seems that by transplanting healthy mitochondria, we may be reintroducing something akin to an orchestra conductor—one that helps reorganize and direct the cellular response, modulating what the cell already knows how to do, but perhaps needed additional support to execute effectively.

Sustaining this line of investigation is crucial, as RIRI remains a pressing global health emergency and a leading cause of irreversible blindness. The potential for MT to serve as a transformative, upstream intervention in ischemic retinal disease underscores its clinical relevance and the urgency of advancing this field.

Limitations and Future Directions

The ARPE-19 cell line serves as a practical and reproducible model for studying RPE function, especially when enhanced through targeted maturation protocols. In our study, we implemented a proven protocol, promoting a cobblestone morphology and more physiologically relevant behavior, aligning ARPE-19 cells closer to native RPE. However, the immortalized nature of ARPE-19 may introduce altered gene expression, limited polarization, and reduced expression of certain RPE-specific markers. These limitations can compromise the fidelity of key processes such as apoptosis, oxidative response, and mitochondrial function. The in vitro environment also lacks the complex retinal microarchitecture and cell-cell interactions present in vivo. Thus, while ARPE-19 cells offer a valuable and scalable model, results should be cautiously interpreted and validated with more physiologically relevant systems.

Although our findings did not directly assess size-function relationships, mitochondrial size alone is not a reliable indicator of viability or activity. Functional readouts such as membrane potential (e.g., JC-1 staining), oxygen consumption rate (Seahorse), would be more informative. Future studies may explore whether isolating mitochondria by size via microfiltration or flow cytometry reveals distinct activity profiles, though caution must be taken to avoid damaging mitochondria in the process ad describing the biological rationale based on cell type. Regarding quality between batches, we acknowledge the limitations of relying solely on size/count metrics. Future studies could incorporate enzymatic activity assays (e.g., citrate synthase), mitochondrial membrane potential assays, or total protein content quantification (e.g., BCA assay) to further confirm isolate quality. Flow cytometry was avoided to preserve viability, but non-invasive quality metrics would enhance reproducibility in future translational applications.

As discussed, our H_2O_2 protocol as a surrogate for RIRI testing in vivo, remains valid for initial mechanistic exploration, though future integration with more complex models will be critical for validating the therapeutic relevance of MT.

After the shown effect of MT in our model, the question arouses that if functional mitochondria truly mediate protection, then non-functional ones should fail to rescue cells Including such a control could help rule out any artifactual benefit from simply adding mitochondrial components or proteins. It addresses the concern that perhaps some mitochondrial membrane fragments or mitochondrial DNA could have non-specific effects on cells (for instance, by stimulating minor stress responses or uptake of mitochondrial protein that somehow aids cells). A control with inactivated mitochondria tests this directly. In the broader literature, investigators have indeed used this strategy, where for example MT in UV-irradiated cells and included mitochondria that were heat-inactivated, ultrasonically ruptured, or freeze-thawed as controls. The intact mitochondria rescued cell viability, whereas the non-functional mitochondria did not, leading the authors to conclude that the structural integrity of mitochondria is essential for the protective effect Specifically, they found that neither ATP alone, nor mitochondrial fragments, could replicate the benefit, confirming it required whole, functional organelles.

Following with the transcriptomic analysis, the selection of 1-hour and 4-hour post-transplantation RNA-seq timepoints aimed to capture immediate early transcriptional responses and the onset of adaptive signaling. Our intention was to characterize the first molecular events triggered by oxidative stress and mitochondrial intervention, those most likely to initiate downstream protective or apoptotic pathways. While this early-window approach provides mechanistic insight into the initial cellular decision-making, we acknowledge that it may not fully capture the broader biological context or long-term responses. Looking toward clinical application, particularly in

acute retinal ischemia, therapeutic decisions must often be made within hours. Thus, we prioritized these timepoints to reflect the urgency and dynamics of early intervention. Nevertheless, extending the analysis to later timepoints (12, 24, 48 hours) will be critical in future studies to track reparative processes, sustained gene regulation, and mitochondrial integration.

During RNA-seq analysis, PCA revealed distinct clustering between groups, but some within-group variability was noted. This could stem from subtle differences in mitochondrial uptake, ARPE-19 differentiation status, or sequencing batch effects. While normalization and QC measures were applied, further improvements could include cell synchronization prior to treatment, expanded replicates, and batch correction algorithms in RNA-seq pipelines. Our RNA-seq analysis identified several inflammatory and stress-related pathways, such as IL-17 signaling, TNF activation, and PD-L1 immune modulation, as potentially modulated by MT under oxidative stress. These findings provide compelling molecular hypotheses, but transcriptomic changes alone are not sufficient to establish causality. Functional validation is therefore essential to determine whether the predicted pathways are truly involved in the observed rescue and to understand the mechanisms by which mitochondrial transplantation may exert its effects.

A logical next step involves confirming the expression patterns of key genes and proteins within these pathways, using approaches such as qPCR, Western blotting, or immunoassays. These would help verify whether transcriptional trends translate into protein-level changes under oxidative stress, with and without MT. Further validation can then be pursued through pathway perturbation studies, for example by employing pharmacological inhibitors, receptor blockade, or gene knockdown, to assess whether modulating these pathways influences cellular survival or inflammatory signaling. For example, blocking a candidate pathway that was downregulated by

mitochondria and observing a similar protective effect would strengthen its relevance to the rescue mechanism.

In addition, co-culture systems or phenotypic assays could be employed to test whether mitochondrial therapy influences immune interactions or cell fate decisions, such as apoptosis or necrosis. Measurements of cell bioenergetics such as oxygen consumption, would complement these analyses by revealing whether mitochondrial function is indeed preserved or restored.

Ultimately, while the transcriptomic data suggest that MT alters stress and immune signaling, these results remain correlative. Functional follow-up is necessary to distinguish primary mechanisms from secondary responses. Through a combination of gene/protein validation, pathway manipulation, and phenotypic assays, future studies can confirm whether these predicted pathways are truly mediating the therapeutic effect—and whether they can be targeted in parallel to enhance efficacy. This perspective opens the door to understanding MT not just as a metabolic therapy, but as a dynamic systems-level intervention capable of reestablishing physiological order where chaos once prevailed. Ultimately, this study provides a mechanistic framework for the first steps into translating MT into clinically meaningful retinal therapies.

Bibliography

1. Picard M, Shirihai OS. Mitochondrial signal transduction. Cell Metab. 2022 Nov;34(11):1620–53.

2. Liu X, Kim CN, Yang J, Jemmerson R, Wang X. Induction of Apoptotic Program in Cell-Free Extracts: Requirement for dATP and Cytochrome c. Cell. 1996 Jul;86(1):147–57.

3. Vizioli MG, Liu T, Miller KN, Robertson NA, Gilroy K, Lagnado AB, et al. Mitochondria-to-nucleus retrograde signaling drives formation of cytoplasmic chromatin and inflammation in senescence. Genes Dev. 2020 Mar 1;34(5–6):428–45.

4. Forrester JV, Dick AD, McMenamin PG, Roberts F, Pearlman E. Anatomy of the eye and orbit. In: The Eye [Internet]. Elsevier; 2016 [cited 2025 Mar 18]. p. 1-102.e2. Available from: https://linkinghub.elsevier.com/retrieve/pii/B9780702055546000010

5. Tan LX, Li J, Germer CJ, Lakkaraju A. Analysis of mitochondrial dynamics and function in the retinal pigment epithelium by high-speed high-resolution live imaging. Front Cell Dev Biol. 2022;10:1044672.

6. Campbell JP, Zhang M, Hwang TS, Bailey ST, Wilson DJ, Jia Y, et al. Detailed Vascular Anatomy of the Human Retina by Projection-Resolved Optical Coherence Tomography Angiography. Sci Rep. 2017 Feb 10;7(1):42201.

7. Remington LA, editor. Clinical anatomy and physiology of the visual system. 3rd ed. St. Louis: Elsevier/Butterworth-Heinemann; 2012. 292 p.

8. Mitra AK. Ocular transporters and receptors: their role in drug delivery. Oxford: Woodhead publ; 2013. (Woodhead publishing series in biomedicine).

9. Tong Y, Zhang Z, Wang S. Role of Mitochondria in Retinal Pigment Epithelial Aging and Degeneration. Front Aging. 2022 Jul 15;3:926627.

10. Ji MH, Kreymerman A, Belle K, Ghiam BK, Muscat SR, Mahajan VB, et al. The Present and Future of Mitochondrial-Based Therapeutics for Eye Disease. Transl Vis Sci Technol. 2021 Jul 7;10(8):4.

11. Heyck M, Bonsack B, Zhang H, Sadanandan N, Cozene B, Kingsbury C, et al. The brain and eye: Treating cerebral and retinal ischemia through mitochondrial transfer. Exp Biol Med. 2019 Nov;244(16):1485–92.

12. Simó R, Villarroel M, Corraliza L, Hernández C, Garcia-Ramírez M. The Retinal Pigment Epithelium: Something More than a Constituent of the Blood-Retinal Barrier—Implications for the Pathogenesis of Diabetic Retinopathy. J Biomed Biotechnol. 2010;2010:1–15.

13. Pollreisz A, Neschi M, Sloan KR, Pircher M, Mittermueller T, Dacey DM, et al. Atlas of Human Retinal Pigment Epithelium Organelles Significant for Clinical Imaging. Investig Opthalmology Vis Sci. 2020 Jul 10;61(8):13.

14. Simó R, Hernández C. Neurodegeneration in the diabetic eye: new insights and therapeutic perspectives. Trends Endocrinol Metab. 2014 Jan;25(1):23–33.

15. Zheng Y, Yang J, Li X, Qi L, Zheng Z, Kong J, et al. Mitochondria at the crossroads: Quality control mechanisms in neuronal senescence and neurodegeneration. Neurobiol Dis. 2025 May;208:106862.

16. McCully JD, Del Nido PJ, Emani SM. Mitochondrial transplantation: the advance to therapeutic application and molecular modulation. Front Cardiovasc Med. 2023 Dec 15;10:1268814.

17. Kalogeris T, Baines CP, Krenz M, Korthuis RJ. Cell Biology of Ischemia/Reperfusion Injury. In: International Review of Cell and Molecular Biology [Internet]. Elsevier; 2012 [cited 2025 Mar 5]. p. 229–317. Available from: https://linkinghub.elsevier.com/retrieve/pii/B9780123943095000067

18. Slezak J, Tribulova N, Pristacova J, Uhrik B, Thomas T, Khaper N, et al. Hydrogen peroxide changes in ischemic and reperfused heart. Cytochemistry and biochemical and X-ray microanalysis. Am J Pathol. 1995 Sep;147(3):772–81.

19. Immunological Landscape of Retinal Ischemia-Reperfusion Injury: Insights into Resident and Peripheral Immune Cell Responses. Aging Dis [Internet]. 2024 [cited 2025 Mar 4]; Available from: https://www.aginganddisease.org/EN/10.14336/AD.2024.0129

20. Fang SY, Roan JN, Lee JS, Chiu MH, Lin MW, Liu CC, et al. Transplantation of viable mitochondria attenuates neurologic injury after spinal cord ischemia. J Thorac Cardiovasc Surg. 2021 May;161(5):e337–47.

21. Zhang Y, Cho CH, Atchaneeyasakul L ongsri, McFarland T, Appukuttan B, Stout JT. Activation of the Mitochondrial Apoptotic Pathway in a Rat Model of Central Retinal Artery Occlusion. Investig Opthalmology Vis Sci. 2005 Jun 1;46(6):2133.

22. Osborne NN, Casson RJ, Wood JPM, Chidlow G, Graham M, Melena J. Retinal ischemia: mechanisms of damage and potential therapeutic strategies. Prog Retin Eye Res. 2004 Jan;23(1):91–147.

23. Babikian V, Wijman CAC, Koleini B, Malik SN, Goyal N, Matjucha ICA. Retinal Ischemia and Embolism. Cerebrovasc Dis. 2001;12(2):108–13.

24. Nguyen H, Lee JY, Sanberg PR, Napoli E, Borlongan CV. Eye Opener in Stroke: Mitochondrial Dysfunction and Stem Cell Repair in Retinal Ischemia. Stroke. 2019 Aug;50(8):2197–206.

25. Jiang D, Xiong G, Feng H, Zhang Z, Chen P, Yan B, et al. Donation of mitochondria by iPSC-derived mesenchymal stem cells protects retinal ganglion cells against mitochondrial complex I defect-induced degeneration. Theranostics. 2019;9(8):2395–410.

26. Wu SF, Lin CY, Tsai RK, Wen YT, Lin FH, Chang CY, et al. Mitochondrial Transplantation Moderately Ameliorates Retinal Degeneration in Royal College of Surgeons Rats. Biomedicines. 2022 Nov 10;10(11):2883.

27. Liu H, Prokosch V. Energy Metabolism in the Inner Retina in Health and Glaucoma. Int J Mol Sci. 2021 Apr 1;22(7):3689.

28. Medrano CJ, Fox DA. Oxygen consumption in the rat outer and inner retina: Light- and pharmacologically-induced inhibition. Exp Eye Res. 1995 Sep;61(3):273–84.

29. Bill A, Sperber GO. Aspects of oxygen and glucose consumption in the retina: effects of high intraocular pressure and light. Graefe's Arch Clin Exp Ophthalmol. 1990 Jan;228(1):124–7.

30. Jusufovic M, Elsais A, Kerty E. Seven Points That Explain the Lack of Effect from Reperfusion Therapy in Central Retinal Artery Occlusion. Ophthalmol Retina. 2019 Sep;3(9):713–5.

31. Sim, Shaun. Ting, Daniel. Diagnosis and Management of Central Retinal Artery Occlusion. OPHTHALMIC PEARLS [Internet]. 2017 Aug 1; Available from: https://www.aao.org/eyenet/article/diagnosis-and-management-of-crao

32. Hoyek S, Yuan M, Bejjani R, Zacks DN, Miller JW, Vavvas DG, et al. Multimodal Imaging Characteristics and Correlation to Outcomes in Patients With Central Retinal Artery Occlusion Presenting to a Large Academic Center. Am J Ophthalmol. 2025 Feb;270:35–51.

33. Liu Y, Sercombe R, Xie D, Liu K, Chen L. Inhibition of caspase-9 activation and apoptosis is involved in ischemic preconditioning-induced neuroprotection in rat brain. Neurol Res. 2007 Dec;29(8):855–61.

34. Mehta MM, Weinberg SE, Chandel NS. Mitochondrial control of immunity: beyond ATP. Nat Rev Immunol. 2017 Oct;17(10):608–20.

35. Murphy MP, Hartley RC. Mitochondria as a therapeutic target for common pathologies. Nat Rev Drug Discov. 2018 Dec;17(12):865–86.

36. Nakamura Y, Lo EH, Hayakawa K. Placental Mitochondria Therapy for Cerebral Ischemia-Reperfusion Injury in Mice. Stroke. 2020 Oct;51(10):3142–6.

37. Dumitrascu OM, Shen JF, Kurli M, Aguilar MI, Marks LA, Demaerschalk BM, et al. Is Intravenous Thrombolysis Safe and Effective in Central Retinal Artery Occlusion? A Critically Appraised Topic. The Neurologist. 2017 Jul;22(4):153–6.

38. Hayreh SS, Zimmerman MB. Central Retinal Artery Occlusion: Visual Outcome. Am J Ophthalmol. 2005 Sep;140(3):376.e1-376.e.

39. Page PS, Khattar NK, White AC, Cambon AC, Brock GN, Rai SN, et al. Intra-Arterial Thrombolysis for Acute Central Retinal Artery Occlusion: A Systematic Review and Meta-Analysis. Front Neurol. 2018 Feb 21;9:76.

40. Brestoff JR, Singh KK, Aquilano K, Becker LB, Berridge MV, Boilard E, et al. Recommendations for mitochondria transfer and transplantation nomenclature and characterization. Nat Metab. 2025 Jan 16;7(1):53–67.

41. Clemente-Suárez VJ, Martín-Rodríguez A, Yáñez-Sepúlveda R, Tornero-Aguilera JF. Mitochondrial Transfer as a Novel Therapeutic Approach in Disease Diagnosis and Treatment. Int J Mol Sci. 2023 May 16;24(10):8848.

42. Zong Y, Li H, Liao P, Chen L, Pan Y, Zheng Y, et al. Mitochondrial dysfunction: mechanisms and advances in therapy. Signal Transduct Target Ther. 2024 May 15;9(1):124.

43. Emani SM, McCully JD. Mitochondrial transplantation: applications for pediatric patients with congenital heart disease. Transl Pediatr. 2018 Apr;7(2):169–75.

44. Preble JM, Pacak CA, Kondo H, MacKay AA, Cowan DB, McCully JD. Rapid Isolation And Purification Of Mitochondria For Transplantation By Tissue Dissociation And Differential Filtration. J Vis Exp. 2014 Sep 6;(91):51682.

45. Golconda P, Andrade-Medina M, Oberstein A. Subconfluent ARPE-19 Cells Display Mesenchymal Cell-State Characteristics and Behave like Fibroblasts, Rather Than Epithelial Cells, in Experimental HCMV Infection Studies. Viruses. 2023 Dec 28;16(1):49.

46. Hazim RA, Paniagua AE, Tang L, Yang K, Kim KKO, Stiles L, et al. Vitamin B3, nicotinamide, enhances mitochondrial metabolism to promote differentiation of the retinal pigment epithelium. J Biol Chem. 2022 Sep;298(9):102286.

47. Bertero E, O'Rourke B, Maack C. Mitochondria Do Not Survive Calcium Overload During Transplantation. Circ Res. 2020 Mar 13;126(6):784–6.

48. Bodenstein DF, Siebiger G, Zhao Y, Clasky AJ, Mukkala AN, Beroncal EL, et al. Bridging the gap between in vitro and in vivo models: a way forward to clinical translation of mitochondrial transplantation in acute disease states. Stem Cell Res Ther. 2024 May 31;15(1):157.

49. McCully JD, Levitsky S, Del Nido PJ, Cowan DB. Mitochondrial transplantation for therapeutic use. Clin Transl Med. 2016 Mar;5(1):16.

50. Celik A, Orfany A, Dearling J, Del Nido PJ, McCully JD, Bakar-Ates F. Mitochondrial transplantation: Effects on chemotherapy in prostate and ovarian cancer cells in vitro and in vivo. Biomed Pharmacother. 2023 May;161:114524.

51. Lewis TL, Kwon SK, Lee A, Shaw R, Polleux F. MFF-dependent mitochondrial fission regulates presynaptic release and axon branching by limiting axonal mitochondria size. Nat Commun. 2018 Nov 27;9(1):5008.

52. Masuzawa A, Black KM, Pacak CA, Ericsson M, Barnett RJ, Drumm C, et al. Transplantation of autologously derived mitochondria protects the heart from ischemia-reperfusion injury. Am J Physiol Heart Circ Physiol. 2013 Apr 1;304(7):H966-982.

53. Zorov DB, Juhaszova M, Sollott SJ. Mitochondrial Reactive Oxygen Species (ROS) and ROS-Induced ROS Release. Physiol Rev. 2014 Jul;94(3):909–50.

54. Perry SW, Norman JP, Barbieri J, Brown EB, Gelbard HA. Mitochondrial Membrane Potential Probes and the Proton Gradient: A Practical Usage Guide. BioTechniques. 2011 Feb;50(2):98–115.

55. Panda-Jonas S, Jonas JB, Jakobczyk-Zmija M. Retinal Pigment Epithelial Cell Count, Distribution, and Correlations in Normal Human Eyes. Am J Ophthalmol. 1996 Feb;121(2):181–9.

56. Chen X, Tzekov R, Su M, Zhu Y, Han A, Li W. Hydrogen peroxide-induced oxidative damage and protective role of peroxiredoxin 6 protein via EGFR/ERK signaling pathway in RPE cells. Front Aging Neurosci. 2023;15:1169211.

57. Xie Q, Zeng J, Zheng Y, Li T, Ren J, Chen K, et al. Mitochondrial Transplantation Attenuates Cerebral Ischemia-Reperfusion Injury: Possible Involvement of Mitochondrial Component Separation. Braun R, editor. Oxid Med Cell Longev. 2021 Jan;2021(1):1006636.

58. Chen T, Zhu Y, Jia J, Meng H, Xu C, Xian P, et al. Mitochondrial Transplantation Promotes Remyelination and Long-Term Locomotion Recovery following Cerebral Ischemia. Zhang F, editor. Mediators Inflamm. 2022 Sep 15;2022:1–8.

59. Rossi A, Asthana A, Riganti C, Sedrakyan S, Byers LN, Robertson J, et al. Mitochondria Transplantation Mitigates Damage in an In Vitro Model of Renal Tubular Injury and in an Ex Vivo Model of DCD Renal Transplantation. Ann Surg. 2023 Dec 1;278(6):e1313–26.

60. Fisher CR, Ferrington DA. Perspective on AMD Pathobiology: A Bioenergetic Crisis in the RPE. Investig Opthalmology Vis Sci. 2018 Jun 6;59(4):AMD41.

61. Jiang D, Chen FX, Zhou H, Lu YY, Tan H, Yu SJ, et al. Bioenergetic Crosstalk between Mesenchymal Stem Cells and various Ocular Cells through the intercellular trafficking of Mitochondria. Theranostics. 2020;10(16):7260–72.

62. Faghiri Z, Bazan NG. PI3K/Akt and mTOR/p70S6K pathways mediate neuroprotectin D1-induced retinal pigment epithelial cell survival during oxidative stress-induced apoptosis. Exp Eye Res. 2010 Jun;90(6):718–25.

63. Zhou X, Chen H, Wang L, Lenahan C, Lian L, Ou Y, et al. Mitochondrial Dynamics: A Potential Therapeutic Target for Ischemic Stroke. Front Aging Neurosci. 2021 Sep 7;13:721428.

64. Colombe Dromel P, Singh D, Alexander-Katz A, Kurisawa M, Spector M, Young M. Injectable gelatin hydroxyphenyl propionic acid hydrogel protects human retinal progenitor

cells (hRPCs) from shear stress applied during small-bore needle injection. Appl Mater Today. 2020 Jun;19:100602.

65. Bahire KL, Maļuhins R, Bello F, Freitag SV, Jeļisejevs I, Gile R, et al. Hemispheric analysis of mitochondrial Complex I and II activity in the mouse model of ischemia-reperfusion-induced injury. Mitochondrion. 2023 Mar;69:147–58.

66. Zhang Q, Raoof M, Chen Y, Sumi Y, Sursal T, Junger W, et al. Circulating mitochondrial DAMPs cause inflammatory responses to injury. Nature. 2010 Mar;464(7285):104–7.

67. Bretz CA, Savage SR, Capozzi ME, Suarez S, Penn JS. NFAT isoforms play distinct roles in TNFα-induced retinal leukostasis. Sci Rep. 2015 Nov 3;5(1):14963.

68. Bretz CA, Savage S, Capozzi M, Penn JS. The Role of the NFAT Signaling Pathway in Retinal Neovascularization. Investig Opthalmology Vis Sci. 2013 Oct 25;54(10):7020.

69. Nidadavolu LS, Cosardereliogl C, Merino Gomez A, Wu Y, Bopp T, Zhang C, et al. Interleukin-6 Drives Mitochondrial Dysregulation and Accelerates Physical Decline: Insights From an Inducible Humanized IL-6 Knock-In Mouse Model. Duque G, editor. J Gerontol Ser A. 2023 Oct 9;78(10):1740–52.

70. Xu J, Wakai M, Xiong K, Yang Y, Prabakaran A, Wu S, et al. The pro-inflammatory cytokine IL6 suppresses mitochondrial function via the gp130-JAK1/STAT1/3-HIF1α/ERRα axis. Cell Rep. 2025 Mar;44(3):115403.

71. Zhou J, Rasmussen M, Ekström P. cGMP-PKG dependent transcriptome in normal and degenerating retinas: Novel insights into the retinitis pigmentosa pathology. Exp Eye Res. 2021 Nov;212:108752.

72. Arandjelovic S, Ravichandran KS. Phagocytosis of apoptotic cells in homeostasis. Nat Immunol. 2015 Sep;16(9):907–17.

73. Ellisen LW, Ramsayer KD, Johannessen CM, Yang A, Beppu H, Minda K, et al. REDD1, a Developmentally Regulated Transcriptional Target of p63 and p53, Links p63 to Regulation of Reactive Oxygen Species. Mol Cell. 2002 Nov;10(5):995–1005.

74. Kim JY, Kwon YG, Kim YM. The stress-responsive protein REDD1 and its pathophysiological functions. Exp Mol Med. 2023 Sep 1;55(9):1933–44.

75. Foltyn M, Luger AL, Lorenz NI, Sauer B, Mittelbronn M, Harter PN, et al. The physiological mTOR complex 1 inhibitor DDIT4 mediates therapy resistance in glioblastoma. Br J Cancer. 2019 Mar;120(5):481–7.

76. Chaudhary M, Sharma V, Bedi O, Kaur A, Singh TG. SGK-1 Signalling Pathway is a Key Factor in Cell Survival in IschemicInjury. Curr Drug Targets. 2023 Oct;24(14):1117–26.

77. Guerriero I, Monaco G, Coppola V, Orlacchio A. Serum and Glucocorticoid-Inducible Kinase 1 (SGK1) in NSCLC Therapy. Pharmaceuticals. 2020 Nov 22;13(11):413.

78. Yang X, Wu X, Wu K, Yang D, Li Y, Shi J, et al. Correlation of serum- and glucocorticoid-regulated kinase 1 expression with ischemia–reperfusion injury after heart transplantation. Pediatr Transplant. 2015 Mar;19(2):196–205.

79. Rusai K, Prókai Á, Szebeni B, Fekete A, Treszl A, Vannay Á, et al. Role of serum and glucocorticoid-regulated kinase-1 in the protective effects of erythropoietin during renal ischemia/reperfusion injury. Biochem Pharmacol. 2010 Apr;79(8):1173–81.

80. Xie Y, Jiang D, Xiao J, Fu C, Zhang Z, Ye Z, et al. Ischemic preconditioning attenuates ischemia/reperfusion-induced kidney injury by activating autophagy via the SGK1 signaling pathway. Cell Death Dis. 2018 Mar 1;9(3):338.

81. Owens DM, Keyse SM. Differential regulation of MAP kinase signalling by dual-specificity protein phosphatases. Oncogene. 2007 May 14;26(22):3203–13.

82. An N, Bassil K, Al Jowf GI, Steinbusch HWM, Rothermel M, De Nijs L, et al. Dual-specificity phosphatases in mental and neurological disorders. Prog Neurobiol. 2021 Mar;198:101906.

83. Pérez-Sen R, Queipo MJ, Gil-Redondo JC, Ortega F, Gómez-Villafuertes R, Miras-Portugal MT, et al. Dual-Specificity Phosphatase Regulation in Neurons and Glial Cells. Int J Mol Sci. 2019 Apr 23;20(8):1999.

84. Patterson KI, Brummer T, O'brien PM, Daly RJ. Dual-specificity phosphatases: critical regulators with diverse cellular targets. Biochem J. 2009 Mar 15;418(3):475–89.

85. Sun R, Peng M, Xu P, Huang F, Xie Y, Li J, et al. Low-density lipoprotein receptor (LDLR) regulates NLRP3-mediated neuronal pyroptosis following cerebral ischemia/reperfusion injury. J Neuroinflammation. 2020 Dec;17(1):330.

86. Liu L, Jiang Y, Steinle JJ. TNFAIP3 may be key to TLR4-activation of the inflammasome in the retinal vasculature. Exp Eye Res. 2022 Jul;220:109108.

87. Zhou J, Hu M, He M, Wang X, Sun D, Huang Y, et al. TNFAIP3 Interacting Protein 3 Is an Activator of Hippo-YAP Signaling Protecting Against Hepatic Ischemia/Reperfusion Injury. Hepatology. 2021 Oct;74(4):2133–53.

88. Rogers NM, Zammit N, Nguyen-Ngo D, Souilmi Y, Minhas N, Meijles DN, et al. The impact of the cytoplasmic ubiquitin ligase TNFAIP3 gene variation on transcription factor NF-κB activation in acute kidney injury. Kidney Int. 2023 Jun;103(6):1105–19.

Figures

Fig 1. *Confocal Microscopy Assessment of ARPE-19 Cell Morphology at day 0 and 15 of Differentiation in Supplemented Medium: Confocal images (40 x) show the maturation and epithelial-like morphology of ARPE-19 cells cultured at 15 days in nicotinamide-supplemented medium, importantly, a cobblestone monolayer morphology is evident at day 15.*

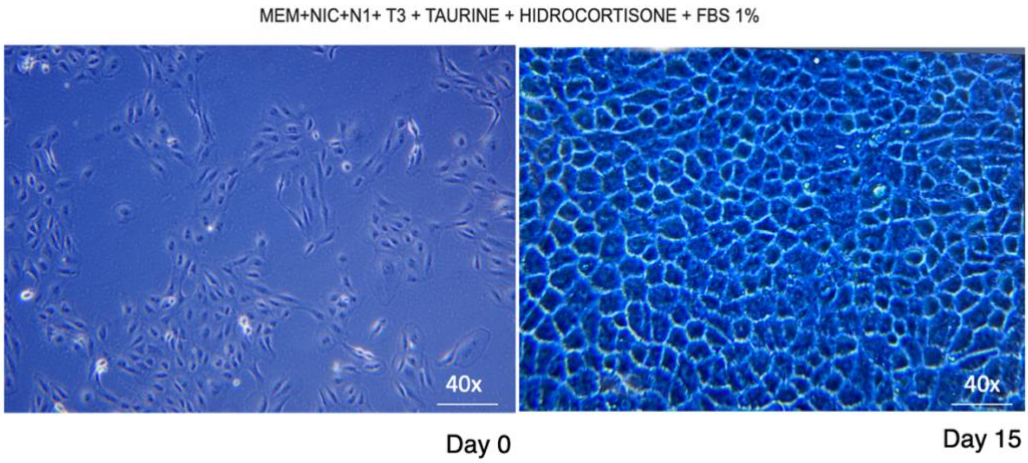


Fig 2. *Mitochondria Isolation: Particle size analysis of mitochondria isolated from 10 million ARPE-19 cells. Range of size distribution was identified at 0.798-0.829 µm (95% CI) and 90% of particles fell below 1 µm (d90= 1.033 µm), with a marked decline in frequency at larger diameters, indicating successful elimination of cellular debris and organelles exceeding mitochondrial dimensions. Minimal residual particles were detected beyond 2 µm.*

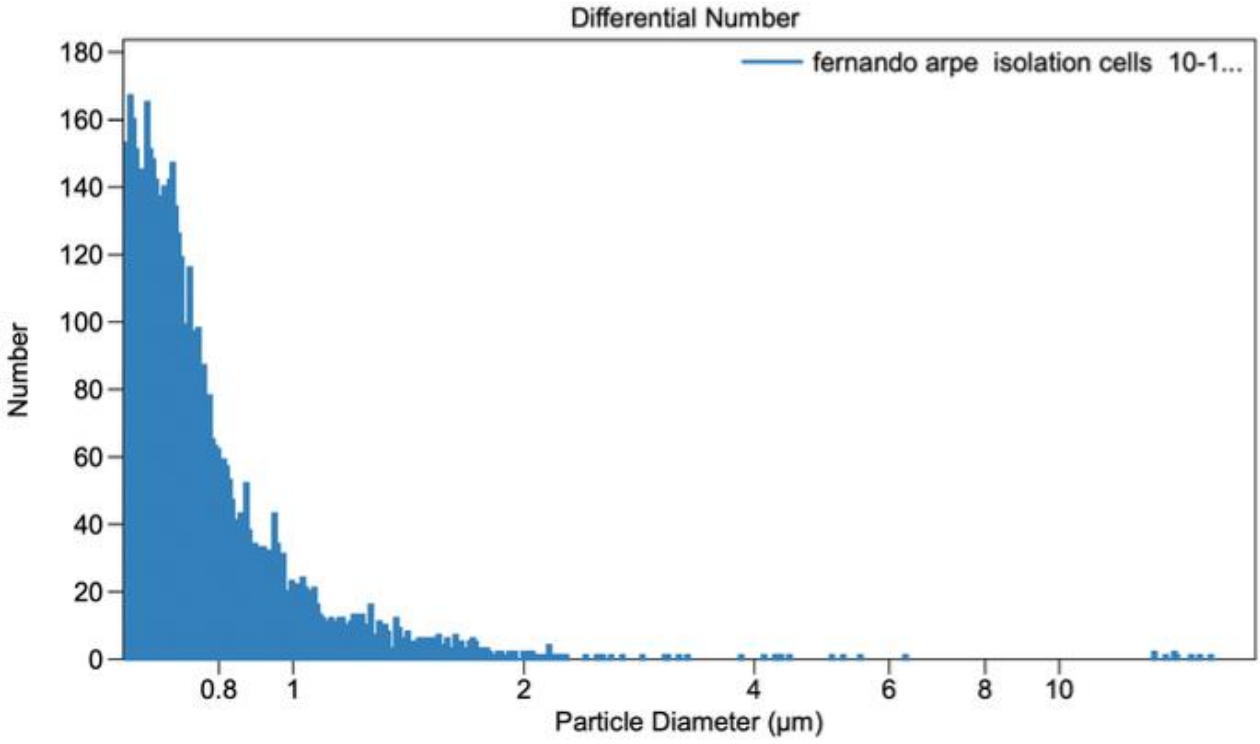


Fig 3. *ATP Production of Isolated Mitochondria in Isolation Buffer and Cell Culture Medium over time (0-180 min.): ATP luminescence assay showing ATP content (µM per 1 x 10^6 mitochondria in Isolation Buffer (solution A) and Cell Culture Medium over time (0-180 min.) All results are shown as mean and standard error of the mean (SE) for n= 6 for each time point. Solution A shown in blue. Cell culture media shown in red. ANOVA and t-test statistical analyses were performed, with significance considered at $p < 0.05$.*

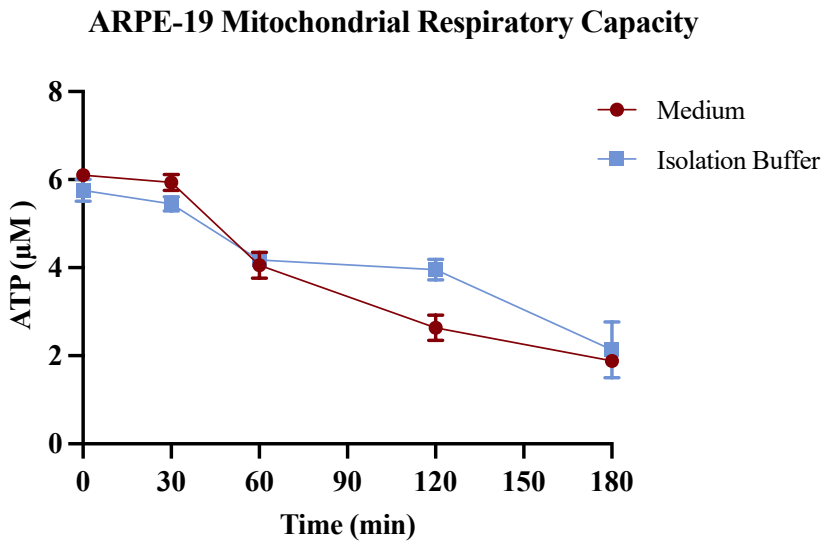
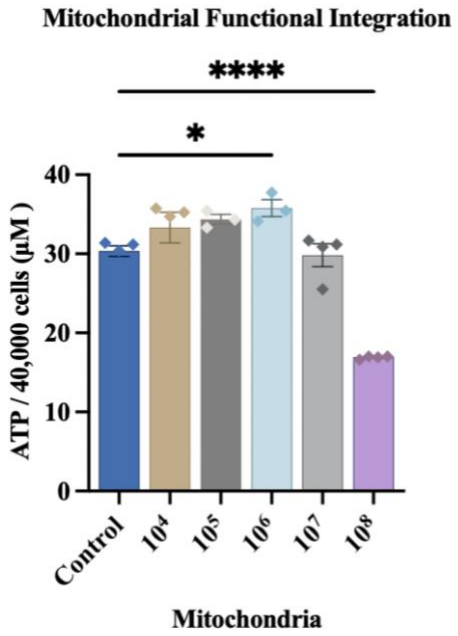


Fig 4. *Uptake and Functional Integration of Transplanted Mitochondria by ARPE-19 Cells and Dose-Dependent ATP Production: A) Differences between external and host mitochondria indicated with white arrows. ANOVA statistical analysis was performed, with significance considered at p < 0.05 (*) and p<0.001 (****). B) Fluorescent imaging of MitoTracker Red-labeled external mitochondria (pink) and MitoTracker Green-labeled host mitochondria (blue), demonstrating mitochondrial uptake and the dose-dependent restoration of ATP production.*

A



B

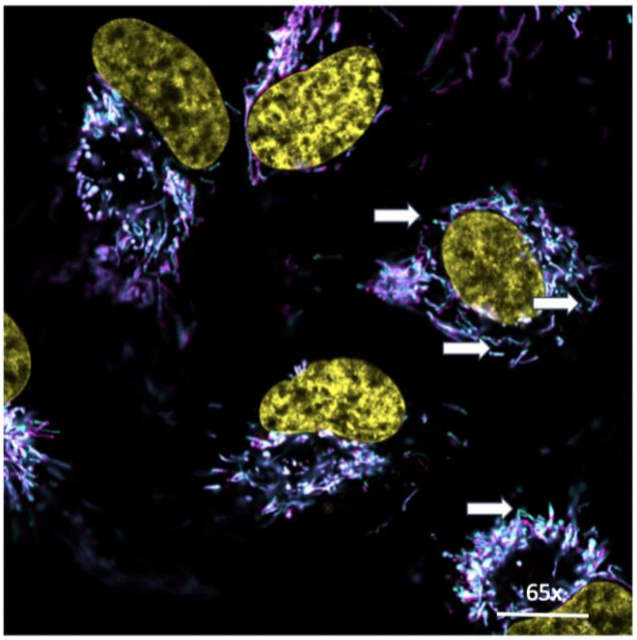


Fig 5. *Colocalization of Transplanted Mitochondria Within the ARPE-19 cells: Confocal images showing the integration of exogenous mitochondria into the host mitochondrial network, with clear colocalization of* ***A-D)*** *transplanted (pink) and* ***B-E)*** *host (green) mitochondria within the cytoplasm. Dotted square shows expanded area, highlighting the* ***C-F)*** *colocalization of transplanted mitochondria within the ARPE-19 mitochondrial network (white arrows).*

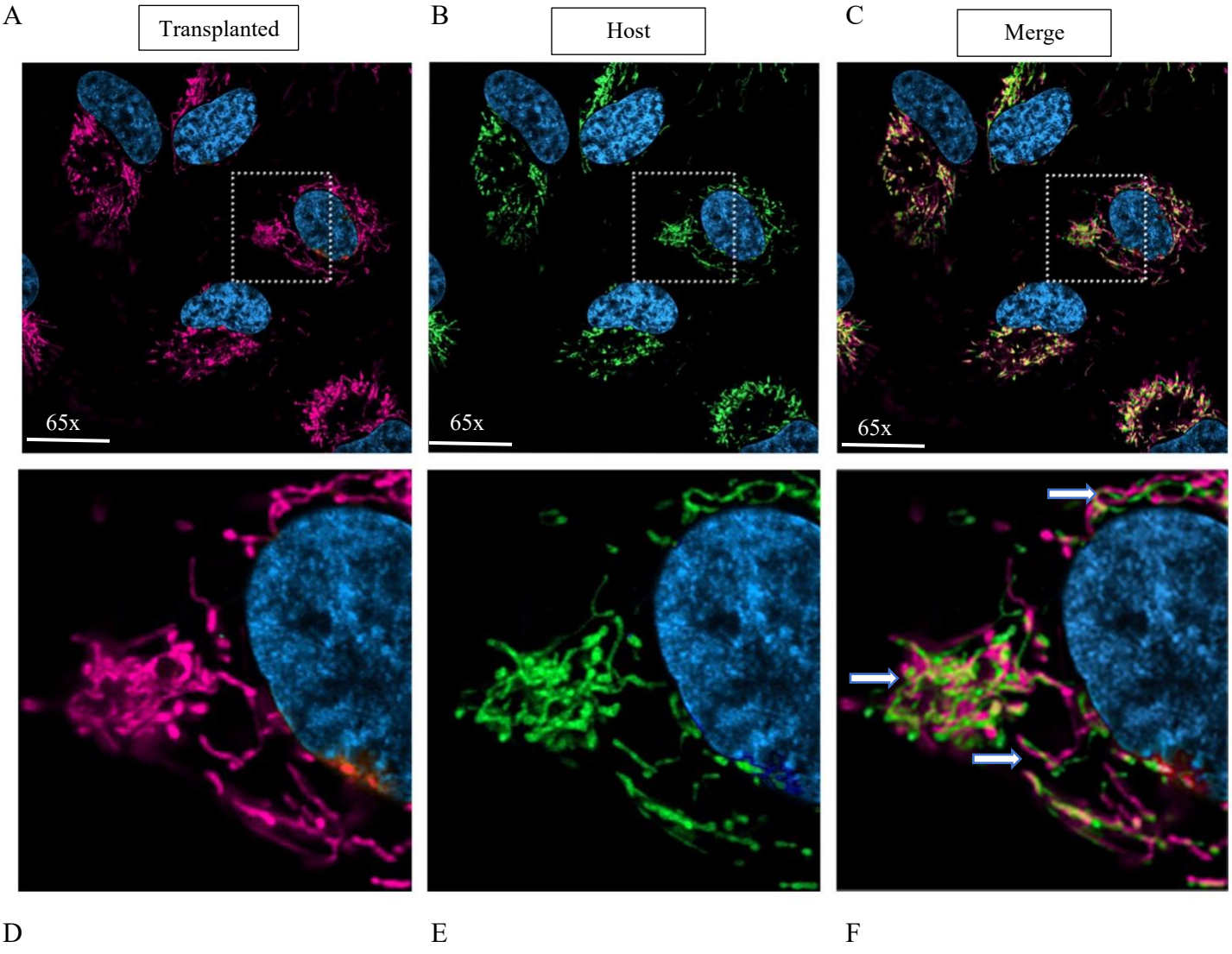


Fig 6. *Z-Stack Imaging Confirming Internalization of Transplanted Mitochondria: Three-dimensional Z-stack confocal images with MitoTracker Red-labeled external mitochondria and MitoTracker Green-labeled host mitochondria confirming that transplanted mitochondria are localized within the cytoplasm of ARPE-19 cells and not superficially attached. White arrows show internalized transplanted mitochondria.*

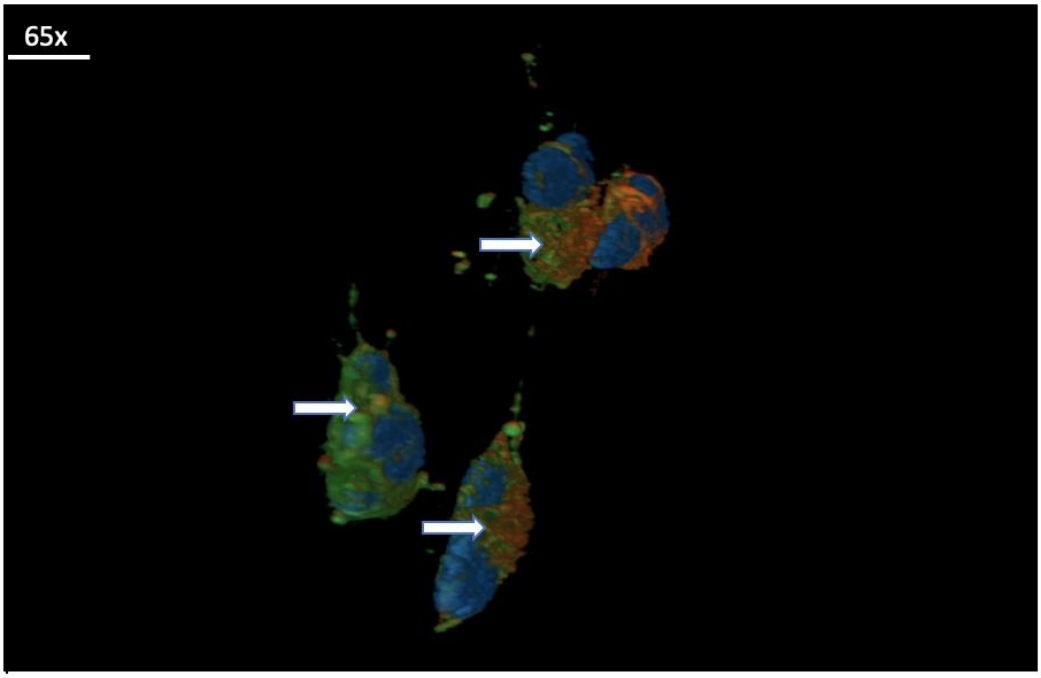
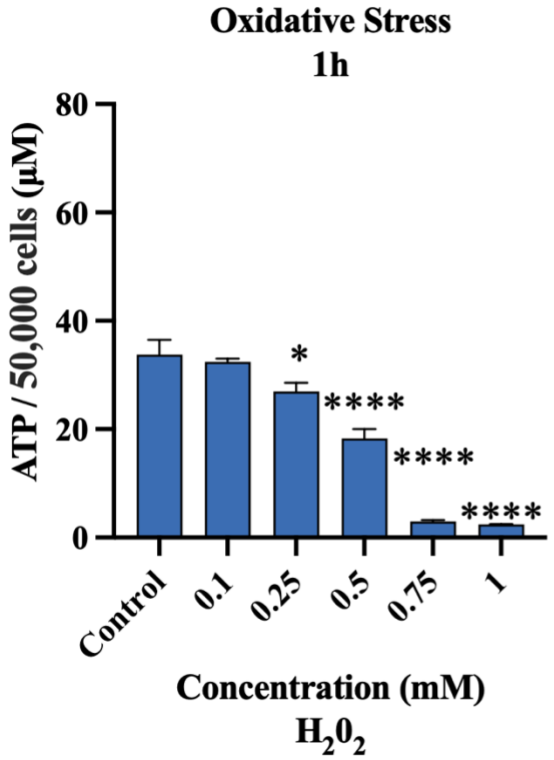


Fig 7. *ATP levels following H_2O_2-induced oxidative stress in ARPE-19 cells at 1(A) and 4 (B) hours.*

ATP content (µM per 50,000 cells) measured by luminescence following exposure to increasing concentrations of hydrogen peroxide (0.1–1 mM) for 1 hour (left, blue) and 4 hours (right, green). A dose- and time-dependent decline in ATP was observed, with significant reductions beginning at 0.25–0.5 mM depending on exposure time. Data represent mean ± SEM from n = 8 wells per condition. Statistical comparisons were performed by one-way ANOVA l. Significance thresholds: p < 0.05 (*), p < 0.01 (**), p < 0.001 (***), p < 0.0001 (****).

A



B

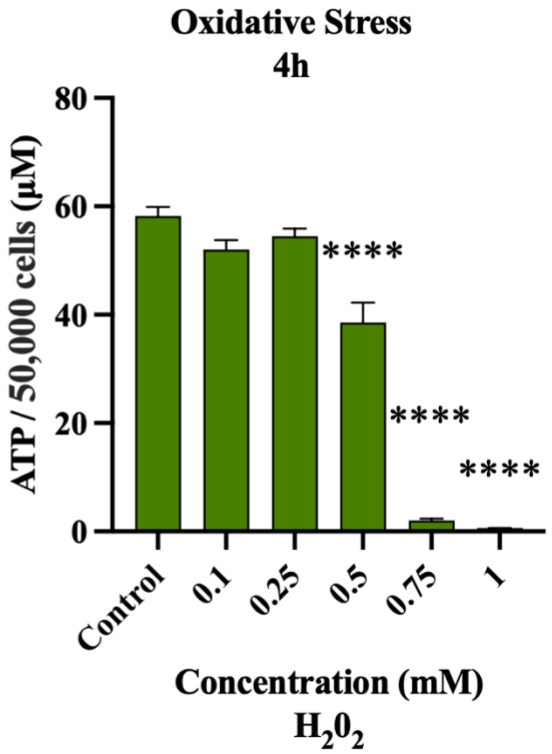


Fig 8. *ATP Production and Mitochondrial Rescue Following Oxidative Stress at 1 and 4 Hours ATP luminescence measurements showing the dose-dependent decline in ATP production/50,000 cells following H_2O_2-induced oxidative stress at concentrations 0.1-1mM and the partial restoration of ATP levels after MT at both 1-hour and 4-hour time points. ANOVA statistical analysis was performed, with significance considered at $p < 0.05$ (*), $p < 0.01$ (**), $p < 0.001$ (**), $p < 0.0001$ (****). All results are shown as mean and SE for n= 8 for each time point.*

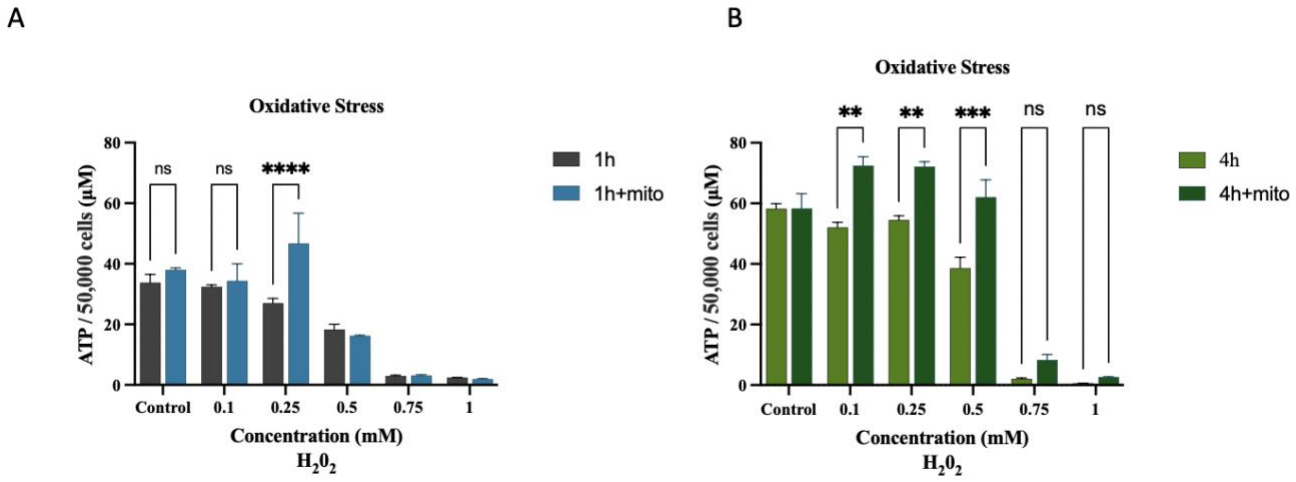


***Fig 9**. Live/Dead Cell Assay Demonstrating the Protective Effect of Mitochondrial Transplantation Under Oxidative Stress: A) Fluorescent images of ARPE-19 cells stained with Calcein AM (live cells, green) and Ethidium Homodimer-1 (dead cells, red) after oxidative stress, highlighting reduced cell death in mitochondria-treated groups. ANOVA statistical analysis was performed, with significance considered at $p < 0.05$ (*) b) percentage of Ethidium Homodimer-1 (EthD-1) positive cells, after 1 hour (left panel) and 4 hours (right panel) of exposure to increasing concentrations of H_2O: Vehicle-treated cells (orange bars) and Mitochondria-transplanted cells (red bars). Data are presented as mean ± standard deviation. Asterisks (*) indicate statistically significant differences between groups set at $p < 0.05$.*

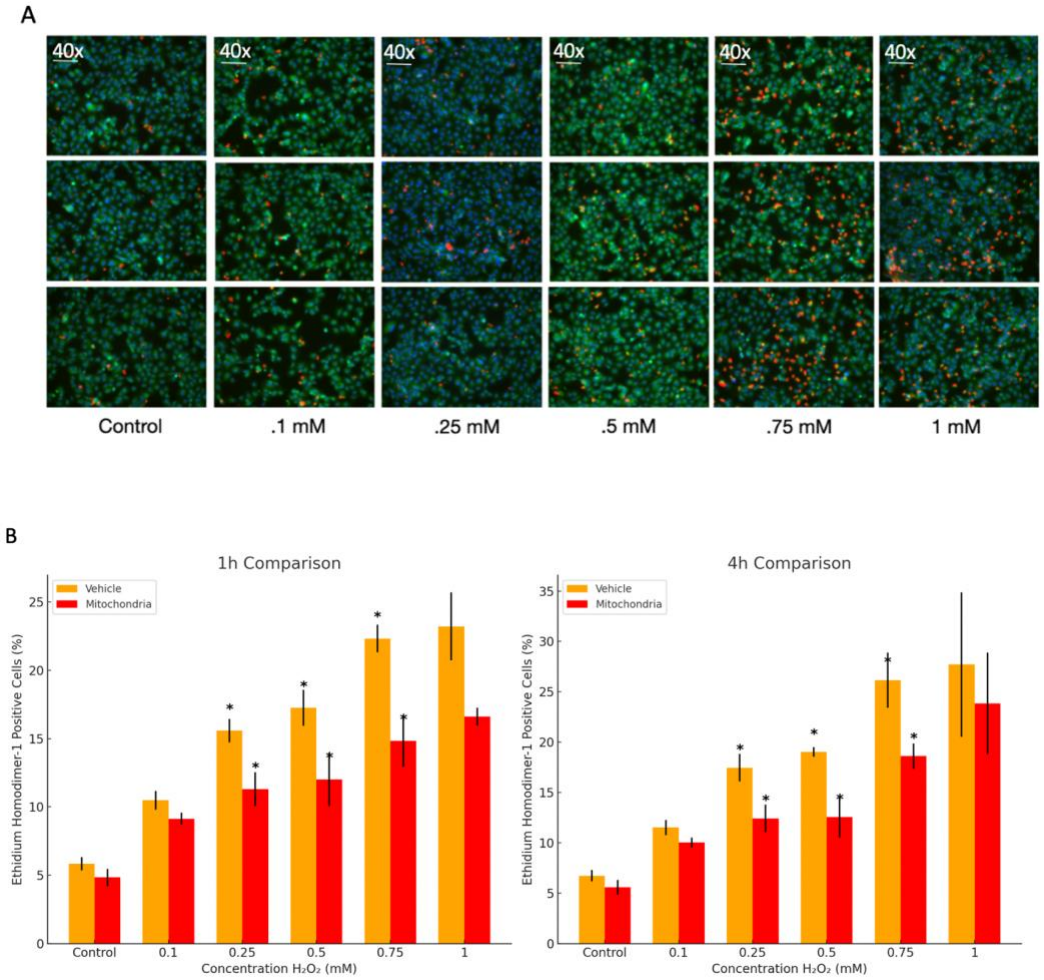


Fig 10. *Hierarchical Clustering Heatmap of Top Differentially Expressed Genes Following Oxidative Stress and Mitochondrial Transplant in ARPE-19 Cells: Heatmap displaying the top differentially expressed genes (Log2 fold change > 1.5, p < 0.05) across ARPE-19 cells exposed to 0.3 mM H_2O_2 for 1 hour and 4 hours, with and without MT. Scale shows green as upregulation and blue as downregulation.*

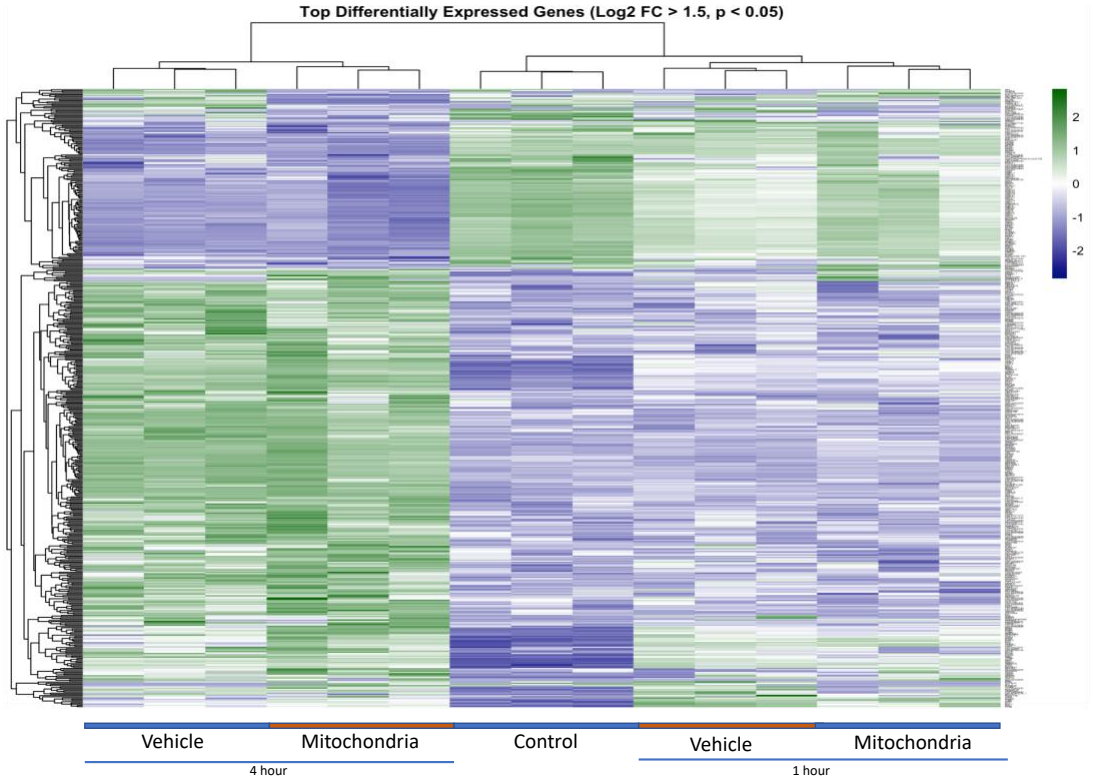


Fig 11. *Principal Component Analysis of Global Gene Expression After 1 and 4 Hours of Oxidative Stress PCA plot showing separation between mitochondrial-treated and untreated control groups, reflecting transcriptomic changes after oxidative stress and MT.*

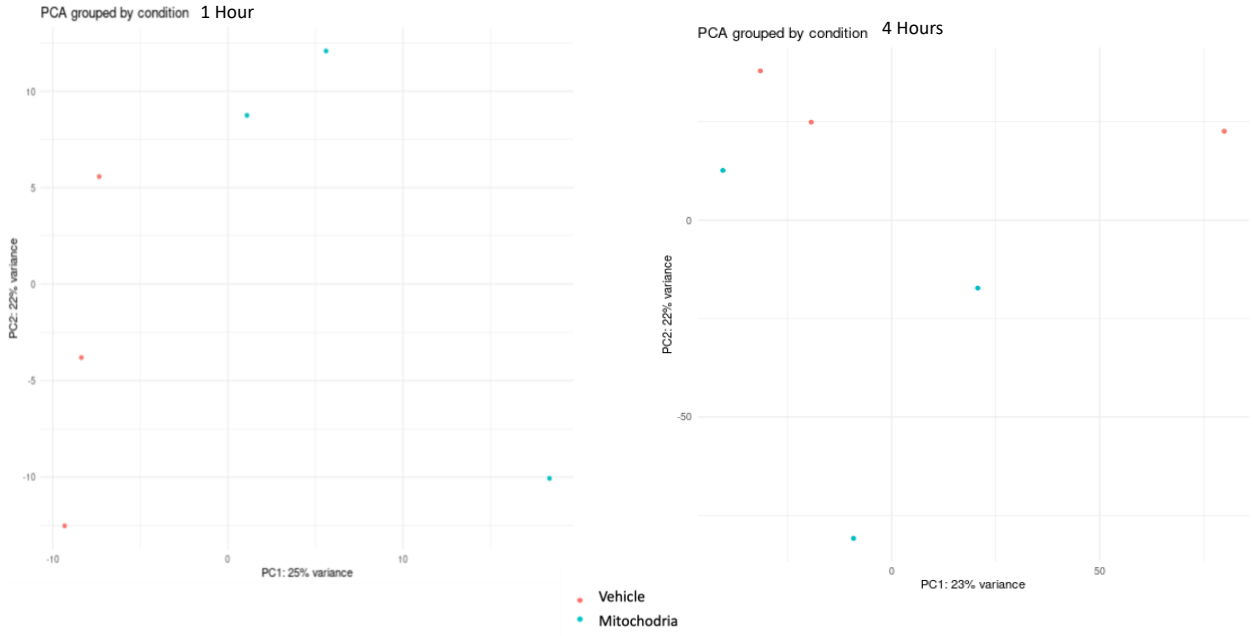


Fig 12. *Volcano Plots of Differentially Expressed Genes Following 1 and Hours of Oxidative Stress: Volcano plots highlighting significantly upregulated and downregulated genes in mitochondrial-treated ARPE-19 cells compared to controls after A) 1-hour H_2O_2 exposure and B) 4-hour H_2O_2 exposure. Y axis represents -$Log_{10}P$ and X axis Log_2 fold change.*

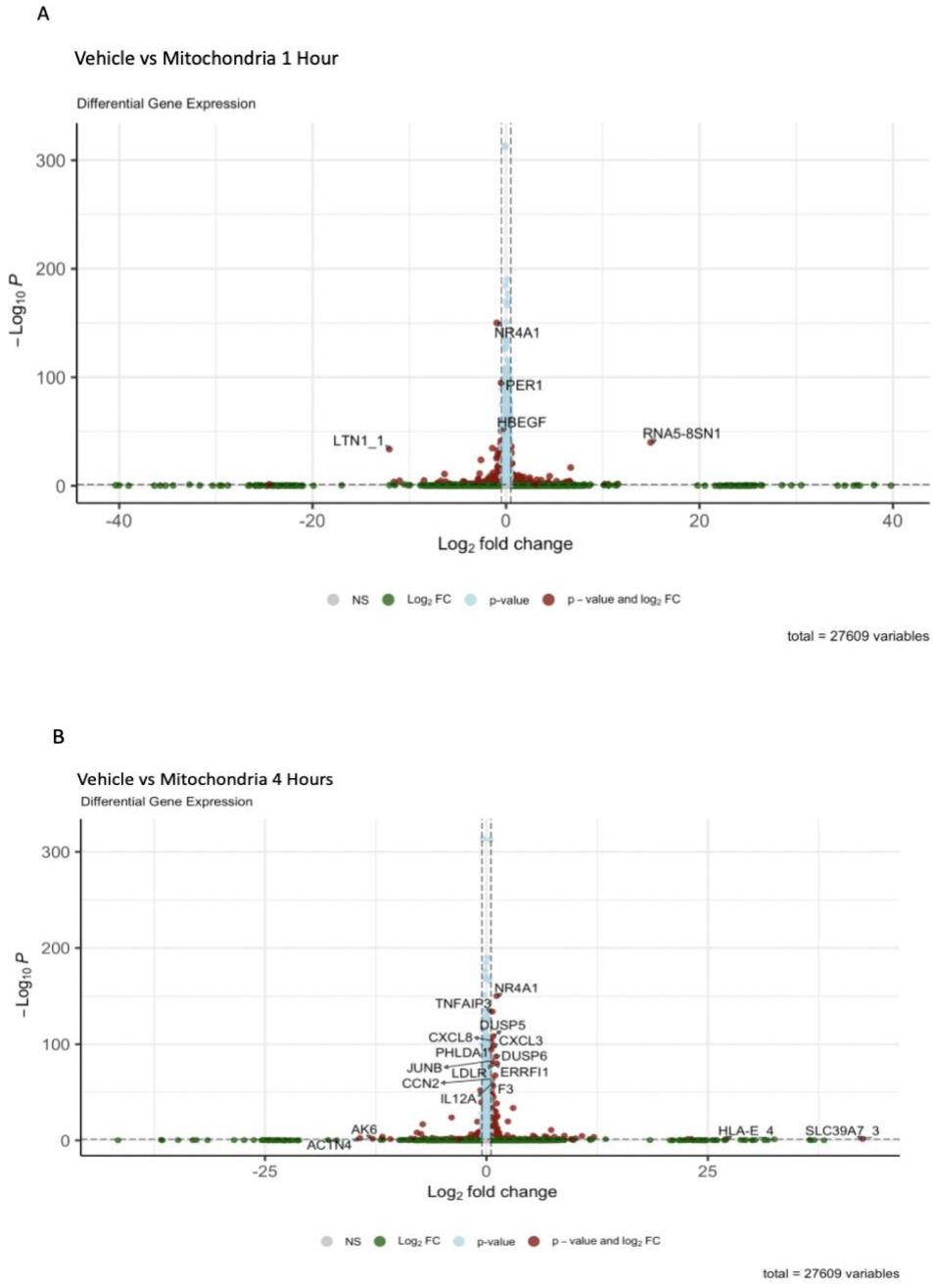


Fig 13. *GO enrichment dot plot of differentially expressed genes following 1-hour oxidative stress and 1 hour mitochondrial transplantation (MT). Dot plot illustrating Gene Ontology (GO) enrichment analysis of biological processes significantly associated with differentially expressed genes between oxidative stress and mitochondrial transplantation treatment at 1 hour. The y-axis lists enriched GO terms, while the x-axis represents the gene ratio (the number of genes associated with a GO term divided by the total number of input genes). Dot size corresponds to the number of genes enriched in each category (Count), and dot color reflects the adjusted p-value (p.adjust), with darker shades indicating higher statistical significance. Terms related to nuclear division, chromosome segregation, and chromatin assembly were among the most enriched categories. Multiple testing correction was applied to compute adjusted p-values.*

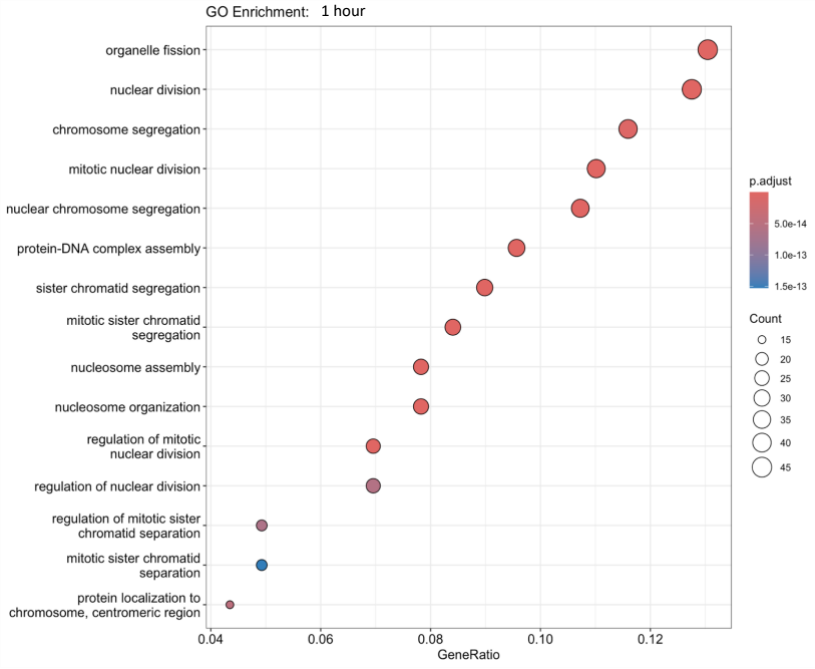


Fig 14. *Cluster Analysis of Mitochondrial-Sensitive Gene Expression Following Oxidative Stress for 1 h and Mitochondrial Transplant in ARPE-19 Cells: DEGs were clustered to identify mitochondrial-sensitive genes — those whose expression was altered by MT. The plot shows gene expression across three conditions: healthy control (shown in blue), untreated oxidative stress (Vehicle shown in yellow), and mitochondrial-transplanted oxidative stress (Mitochondria shown in green). MT partially rescues gene expression, shifting it closer to the healthy baseline.*

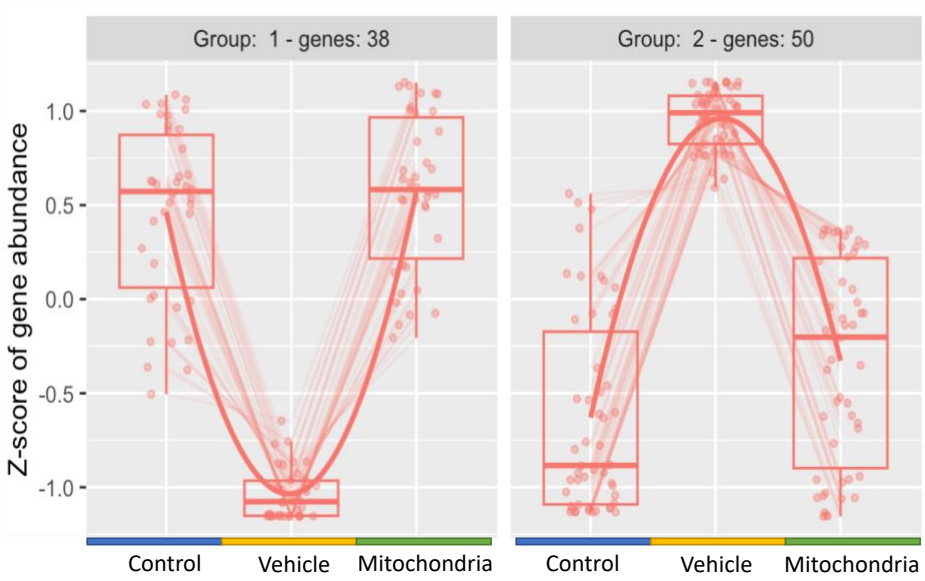


Fig 15. *Heatmap of Mitochondrial-Sensitive Genes in ARPE-19 Cells After Oxidative Stress for 1-hour: Heatmap showing Z-score–normalized expression levels of mitochondrial-sensitive genes across three experimental groups: untreated control (blue bar), oxidative stress vehicle-treated (yellow bar), and mitochondrial-transplanted (green bar) ARPE-19 cells. Genes are shown in the right side and hierarchically clustered by similarity (left dendrogram), allowing visualization of coordinated transcriptional changes. The color scale on the right represents standardized expression values (Z-scores), with red indicating upregulation and blue indicating downregulation. MT shifts the transcriptional profile of stressed cells closer to the control pattern, suggesting partial gene expression rescue.*

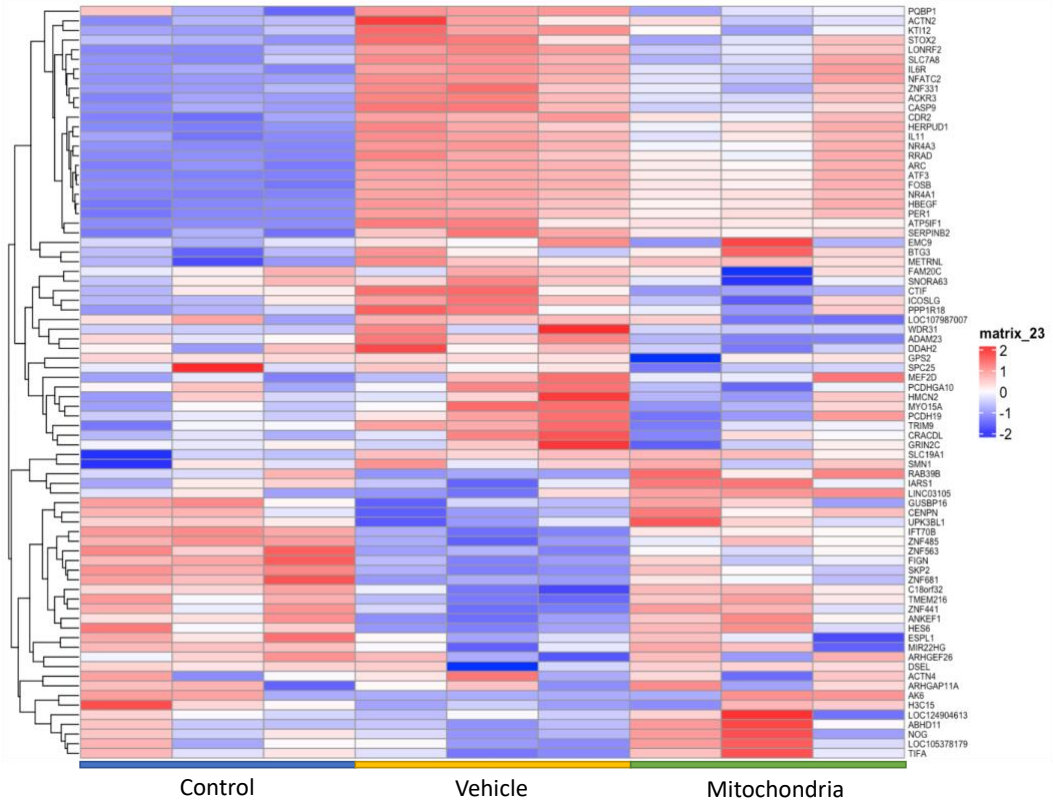


Fig 16. *Top 30 enriched KEGG pathways at 1-hour post-RIRI in mitochondrial-sensitive genes. Dot plot displaying KEGG pathway enrichment of differentially expressed mitochondrial-sensitive genes at 1 hour following RIRI simulation. Pathways are plotted by –log₁₀(p-value) on the x-axis, with each dot representing a pathway. Dot size indicates fold enrichment (range: 4–12), and color intensity reflects statistical significance (darker dots indicate lower p-values). Notable enriched pathways are highlighted with blue arrows. KEGG enrichment analysis was performed on mitochondrial-sensitive gene sets identified at 1-hour post-injury, with multiple testing correction applied to p-values.*

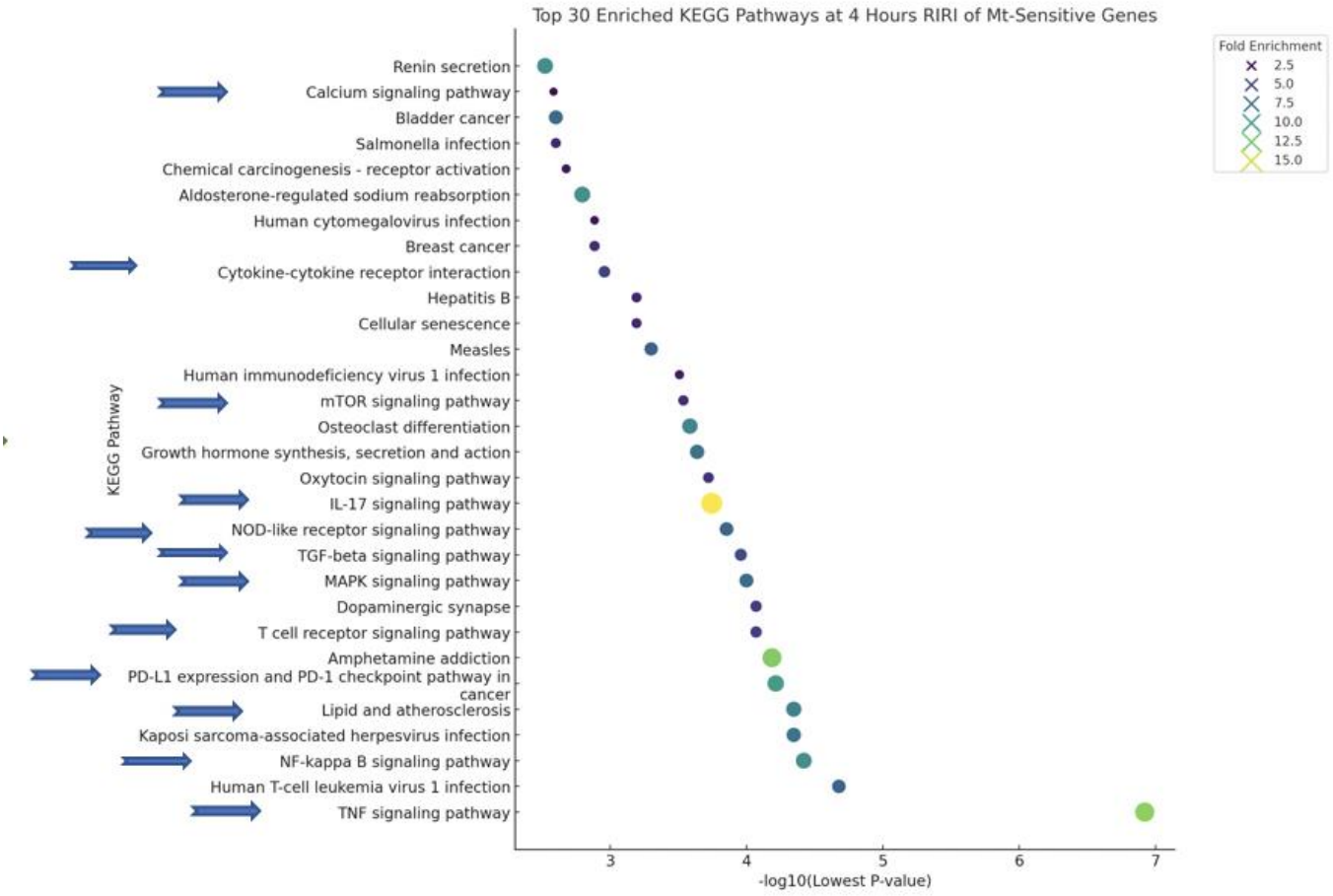


Fig 17*. GO Enrichment Analysis of Differentially Expressed Genes After 4 Hours Oxidative Stress and 1 Hour Mitochondrial Transplant Dot plot displaying Gene Ontology (GO) biological process enrichment for genes differentially expressed between oxidative stress and mitochondrial transplantation treatment, assessed at 4 hours post-injury. The y-axis lists significantly enriched GO terms, while the x-axis represents the gene ratio (the number of genes associated with each term relative to the total number of genes analyzed). Dot size indicates the number of genes contributing to each term (Count), and dot color corresponds to the adjusted p-value (p.adjust), with darker colors indicating greater statistical significance. Terms related to apoptosis, mitochondrial permeability regulation, and muscle and membrane differentiation were among the top enriched processes. Multiple testing correction was applied to determine adjusted p-values.*

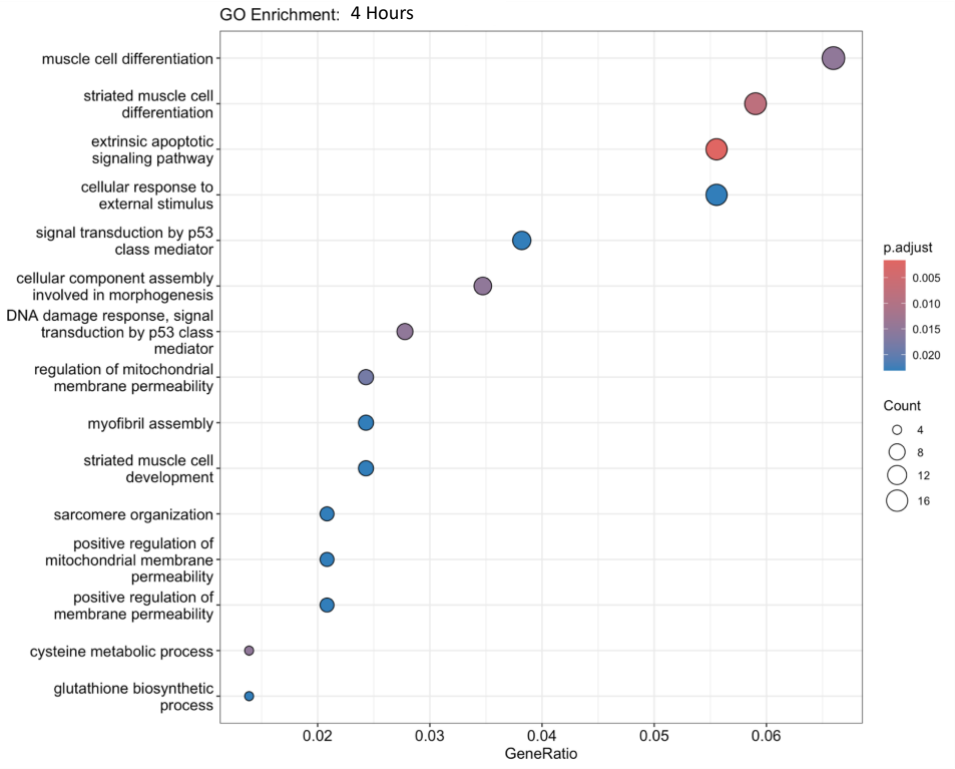


Fig 18. *Cluster Analysis of Mitochondrial-Sensitive Gene Expression Following Oxidative Stress for 4 h and Mitochondrial Transplant in ARPE-19 Cells: DEGs were clustered to identify MT-sensitive genes. The plot shows gene expression across three conditions: healthy control (shown in blue), untreated oxidative stress (Vehicle shown in yellow), and mitochondrial-transplanted oxidative stress (Mitochondria shown in green). MT partially rescues gene expression, shifting it closer to the healthy baseline.*

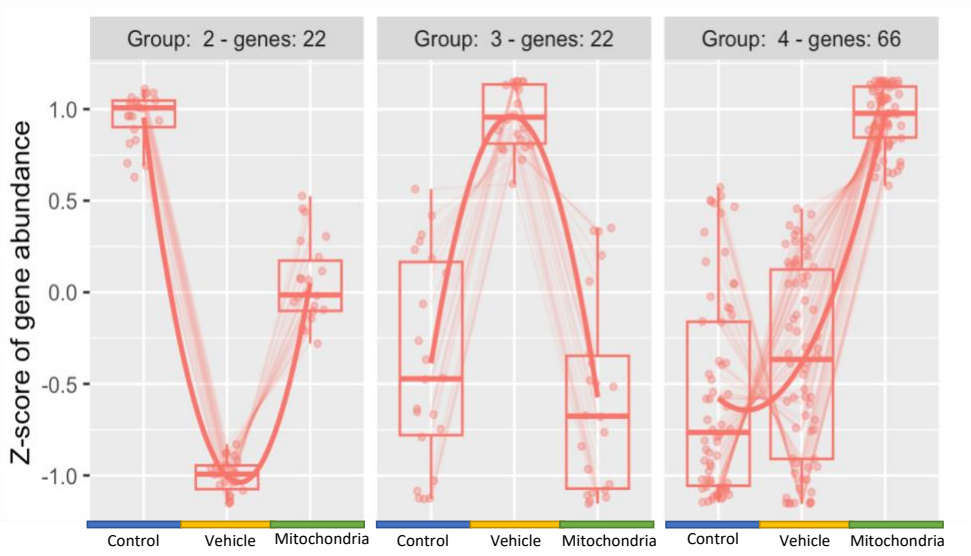


Fig 19. *Heatmap of Mitochondrial-Sensitive Genes in ARPE-19 Cells After Oxidative Stress for 4 hours and Mitochondrial Transplant: Heatmap showing Z-score–normalized expression levels of mitochondrial-sensitive genes across three experimental groups: untreated control (blue bar), oxidative stress vehicle-treated (yellow bar), and mitochondrial-transplanted (green bar) ARPE-19 cells. Genes are shown in the right side and hierarchically clustered by similarity (left dendrogram), allowing visualization of coordinated transcriptional changes. The color scale on the right represents standardized expression values (Z-scores), with red indicating upregulation and blue indicating downregulation. MT shifts the transcriptional profile of stressed cells closer to the control pattern, suggesting partial gene expression rescue.*

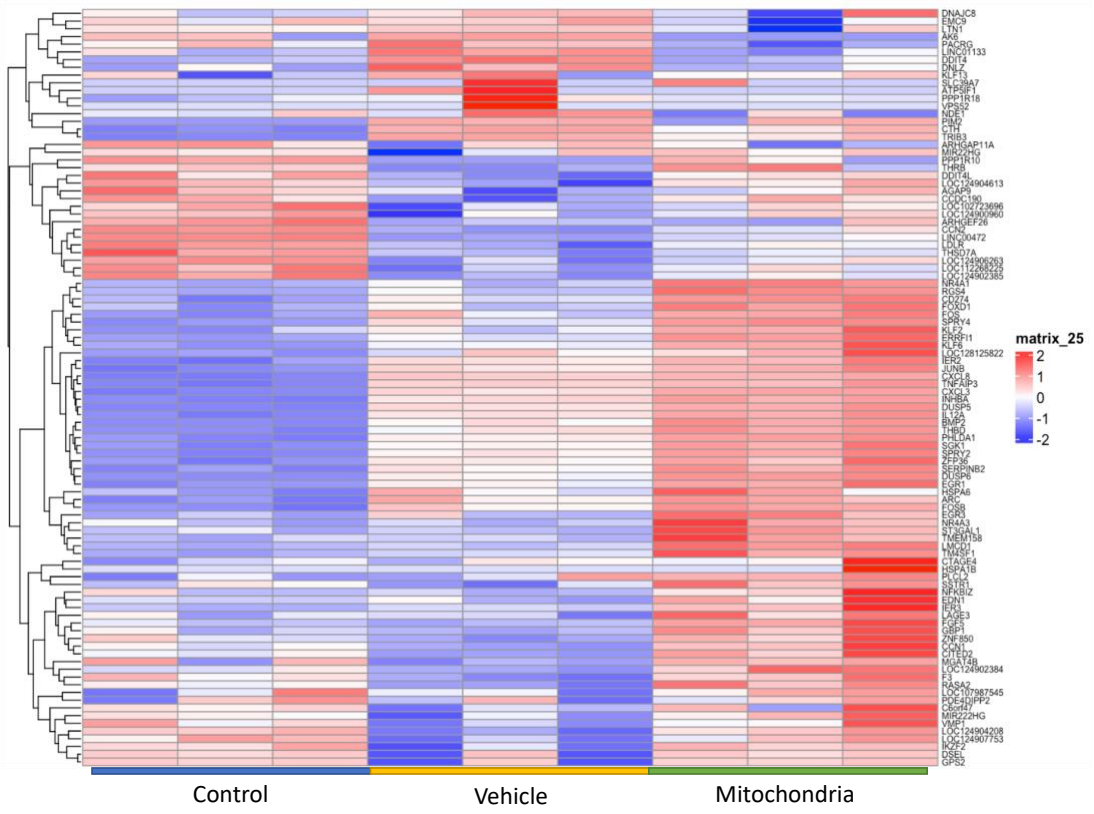


Fig 20. *Top 30 enriched KEGG pathways at 4 hours post-RIRI in mitochondrial-sensitive genes. Dot plot displaying KEGG pathway enrichment of differentially expressed mitochondrial-sensitive genes at 4 hours following RIRI simulation. Pathways are plotted by –log₁₀(p-value) on the x-axis, with each dot representing a pathway. Dot size indicates fold enrichment (ranging from 2.5 to 15.0), while color intensity reflects statistical significance (darker hues represent lower p-values). Notable enriched pathways are highlighted with blue arrows. KEGG enrichment analysis was conducted using mitochondrial-sensitive genes identified at 4 hours post-injury, with p-values adjusted for multiple comparisons.*

